Supplemental Information

Cyanide-Bridged Iron Complexes as Biomimetics of Tri-iron Arrangements in Maturases of the H cluster of the Diiron Hydrogenase

Allen M. Lunsford[†], Christopher C. Beto[†a], Shengda Ding[†], Özlen F. Erdem[δ], Ning Wang[†b], Nattamai Bhuvanesh[†], Michael B. Hall[†] and Marcetta Y. Darensbourg[†]*

[†]*Department of Chemistry, Texas A & M University, College Station, TX 77843, United States*

[δ]*Department of Physics, Middle East Technical University, 06800 Ankara, Turkey*

E-mail: marcetta@chem.tamu.edu

Cyclic Voltammetry

Full Scans

Variable Scan Rates

Scan Reversals

IR Spectrum of Compounds A-D and Cleavage Reactions

NMRs of Compounds A-D

EPR

Crystallographic Images

Tables of Bond Distances and Angles Obtained from the Crystal Structures, IR Frequencies, and EPR Parameters

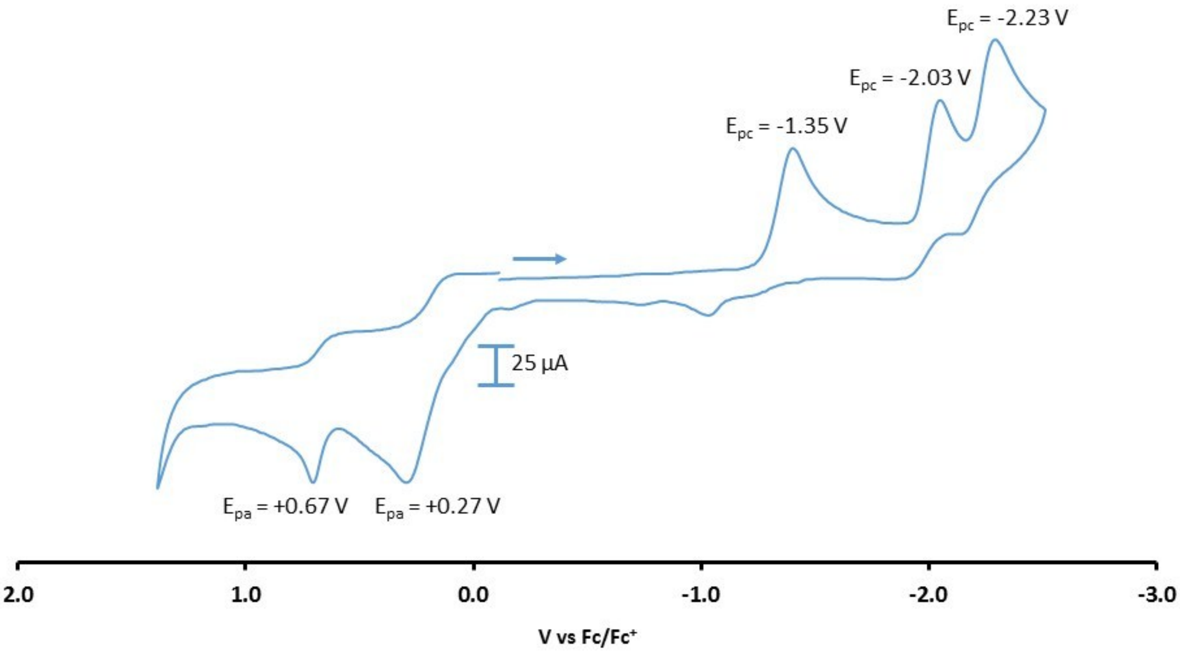

Figure S1. Full scan of Compound **A** at 200 mV/s in MeCN referenced to internal Fc/Fc^{+} = 0.

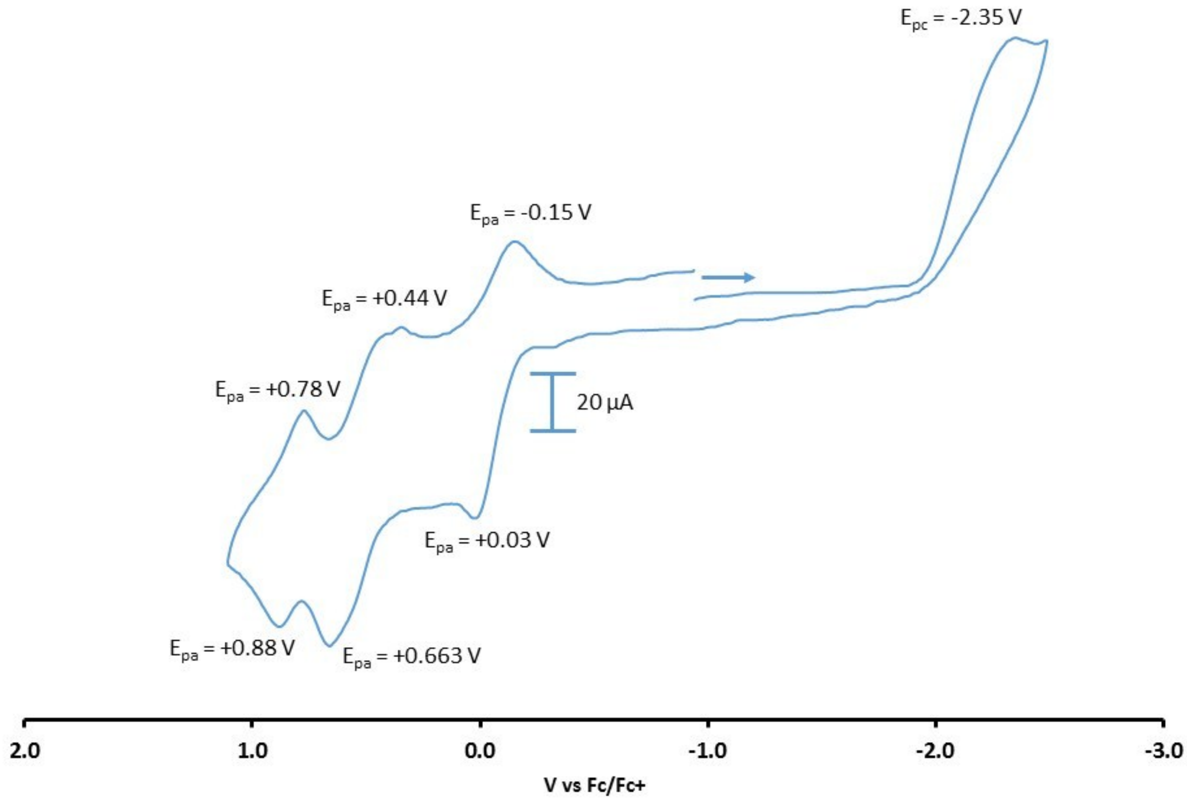

Figure S2. Full scan of Compound **B** at 200 mV/s in DCM referenced to internal $Fc/Fc^+ = 0$.

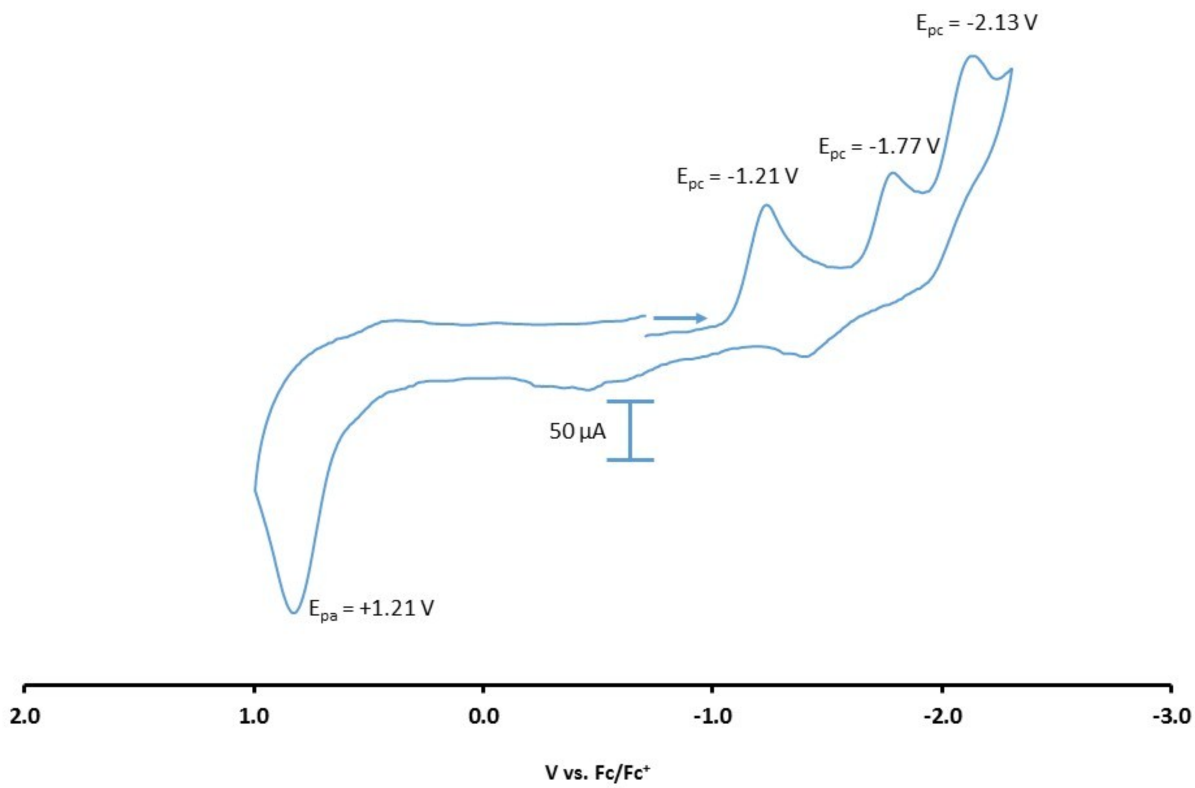

Figure S3. Full scan of Compound **C** at 200 mV/s in DCM referenced to internal $Fc/Fc^{+} = 0$.

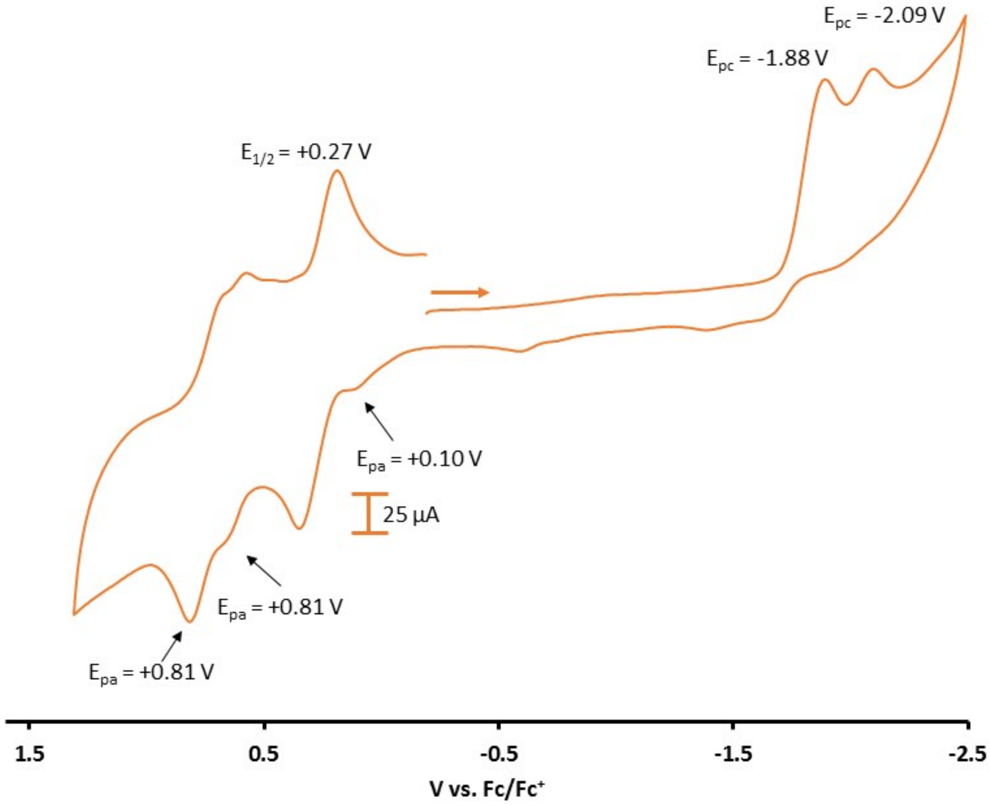

Figure S4. Full scan of Compound **D** at 200 mV/s initiating the scan in the negative direction (top) and the positive direction (bottom) in DCM referenced to internal Fc/Fc$^+$ = 0.

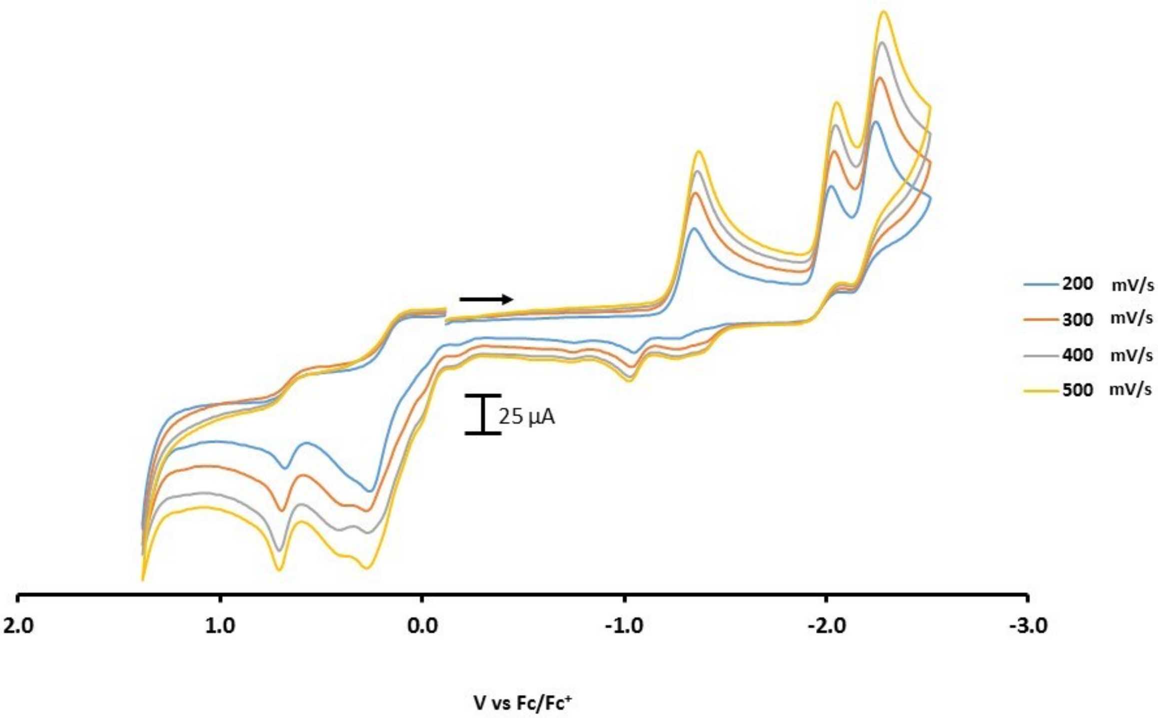

Figure S5. Full scan of Compound **A** at increasing scan rates in MeCN referenced to internal Fc/Fc^{+} = 0.

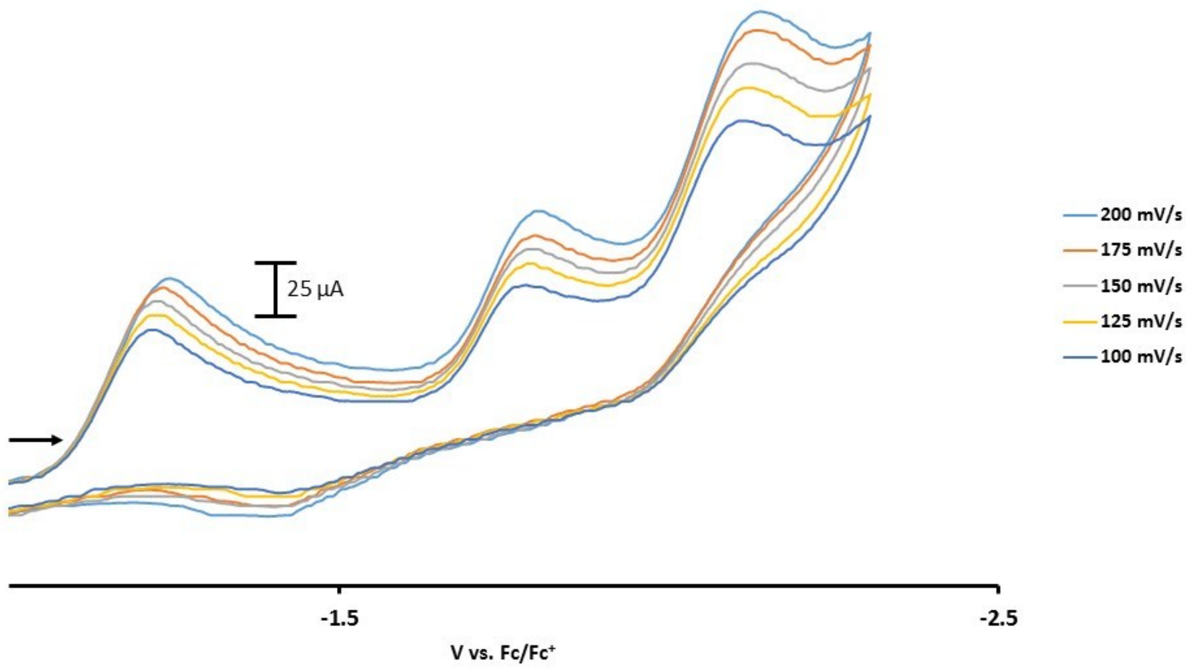

Figure S6. Cathodic region of Compound **C** at increasing scan rates in DCM referenced to internal $Fc/Fc^{+} = 0$.

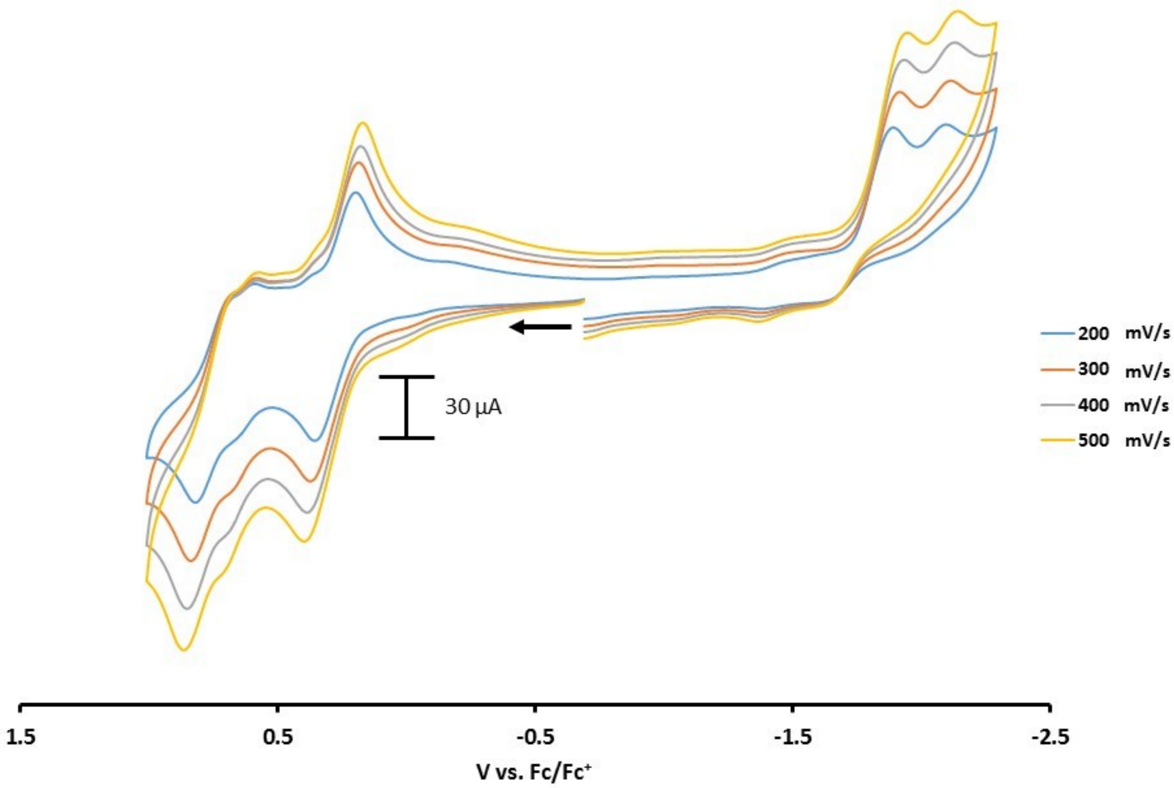

Figure S7. Full scan of Compound **D** at increasing scan rates in DCM referenced to internal Fc/Fc^{+} = 0.

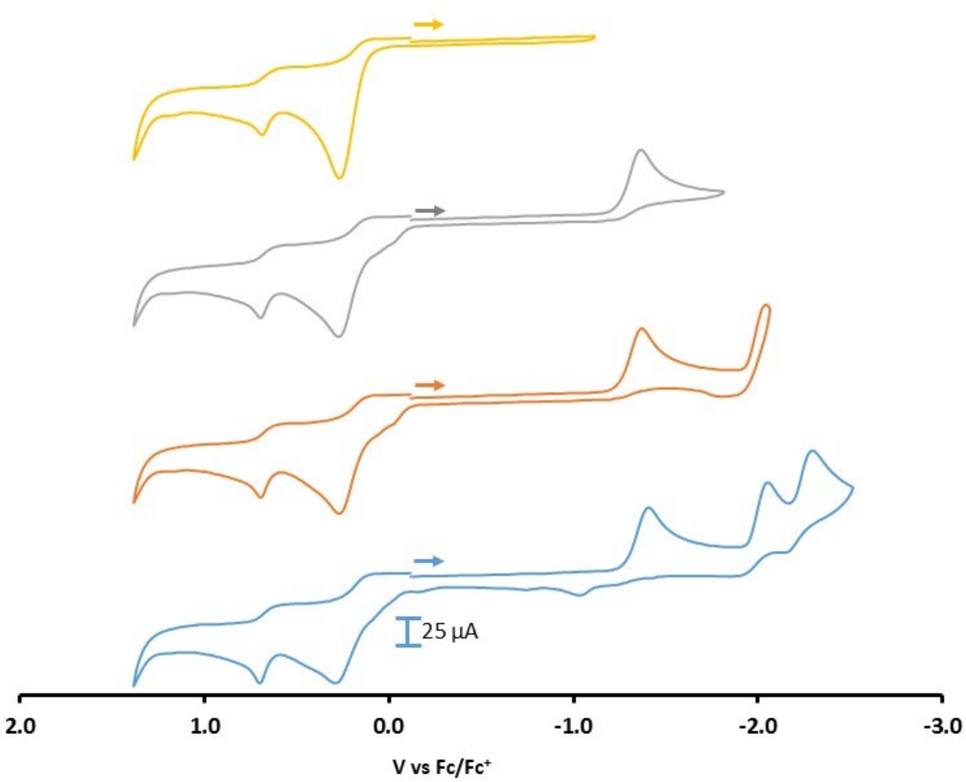

Figure S8. Scan reversals of Compound **A** isolating each reduction event and observing the effect on the anodic region in MeCN referenced to internal $Fc/Fc^{+} = 0$.

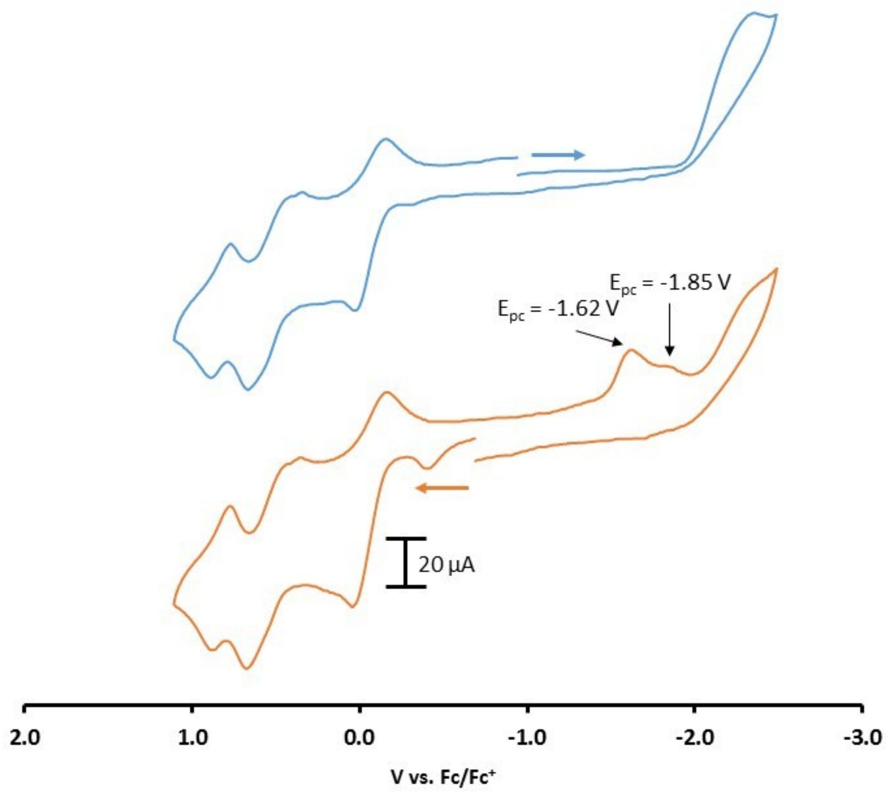

Figure S9. Full scan of Compound **B** at 200 mV/s initiating the scan in the negative direction (top) and the positive direction (bottom) in DCM referenced to internal $Fc/Fc^+ = 0$.

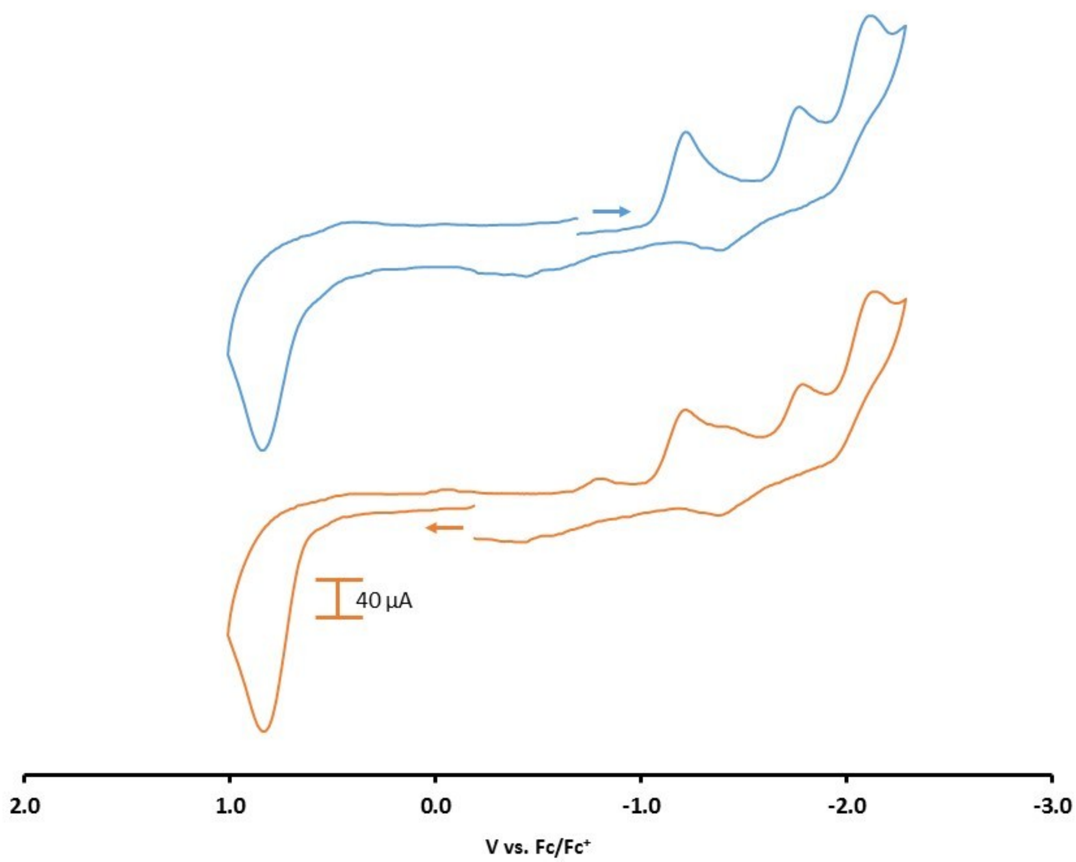

Figure S10. Full scan of Compound **C** at 200 mV/s initiating the scan in the negative direction (top) and the positive direction (bottom) in DCM referenced to internal Fc/Fc^{+} = 0.

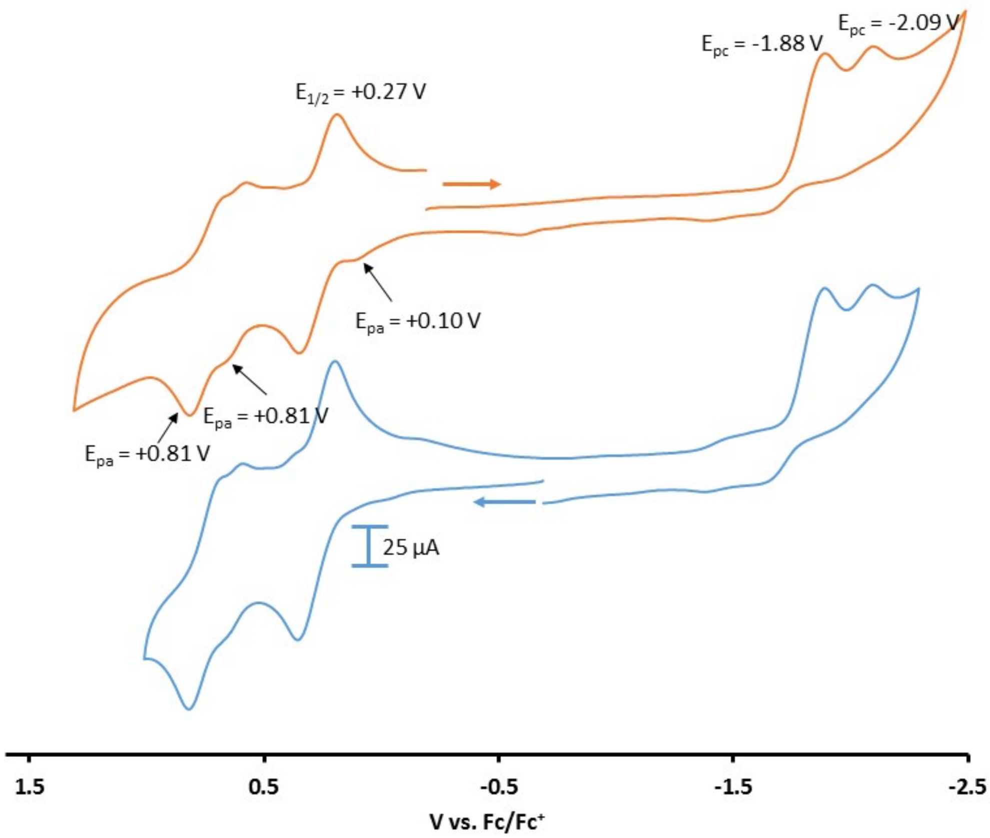

Figure S11. Full scan of Compound **D** at 200 mV/s initiating the scan in the negative direction (top) and the positive direction (bottom) in DCM referenced to internal Fc/Fc^{+} = 0.

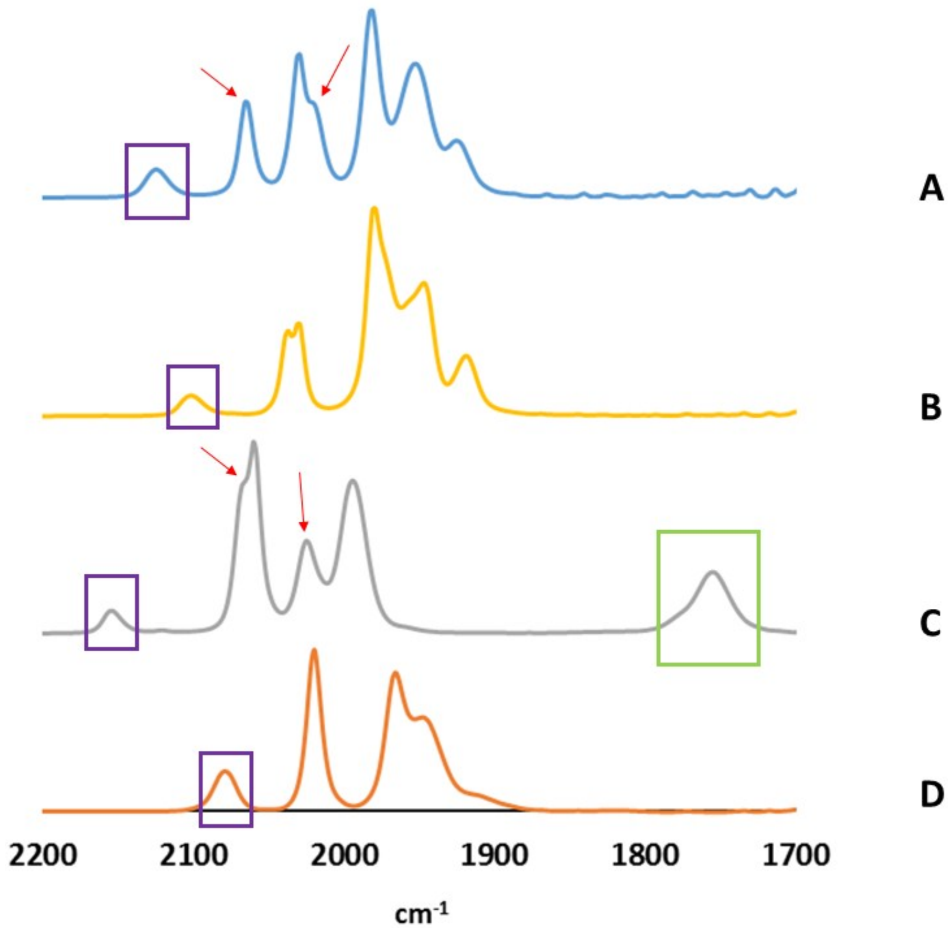

Figure S12. Stacked normalized IR plots of Compounds **A-D** in DCM. Red arrows denote CO stretches on the CpFe unit, purple boxes denote bridging cyanide bands, and the green box denotes the NO stretch.

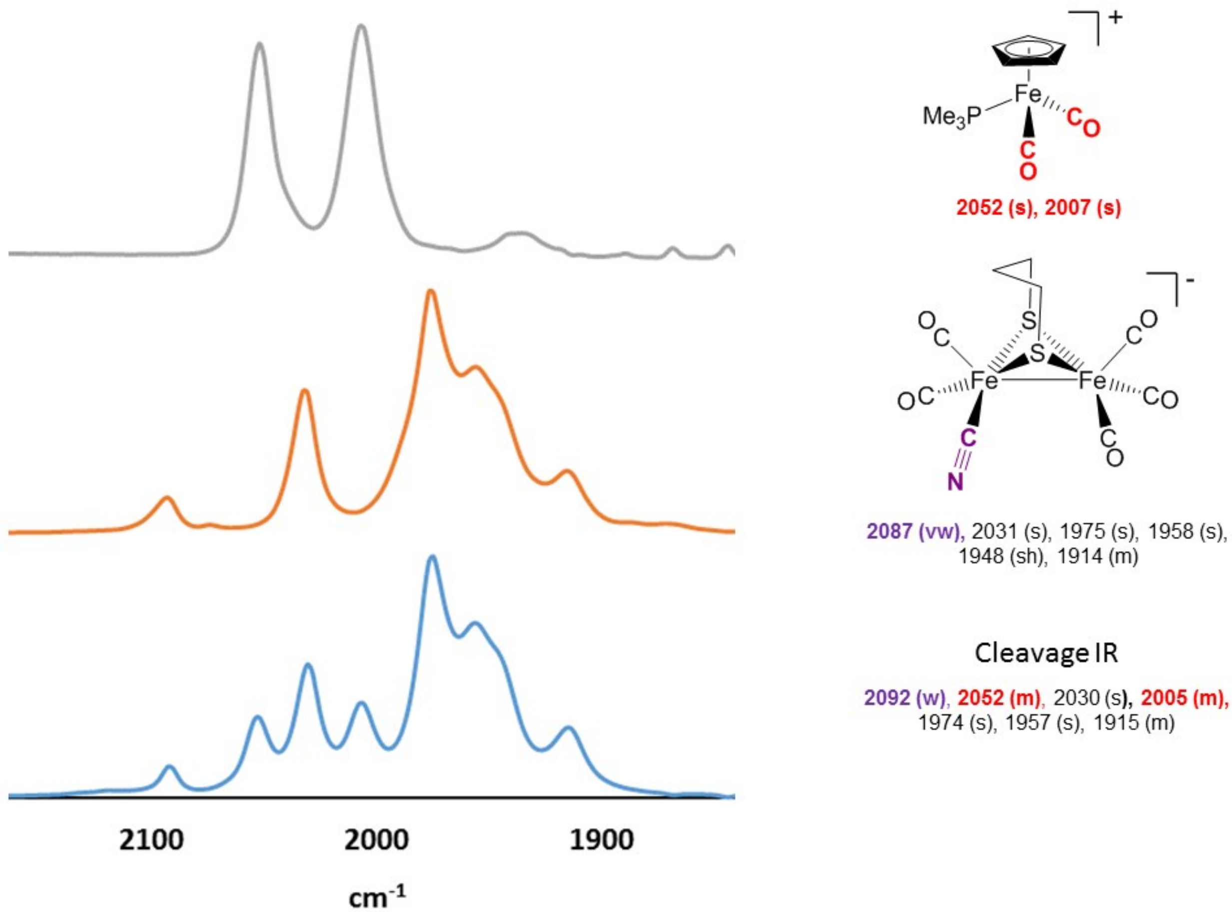

Figure S13. IR spectrum in THF of the cleavage of Compound **A** using PMe_3.

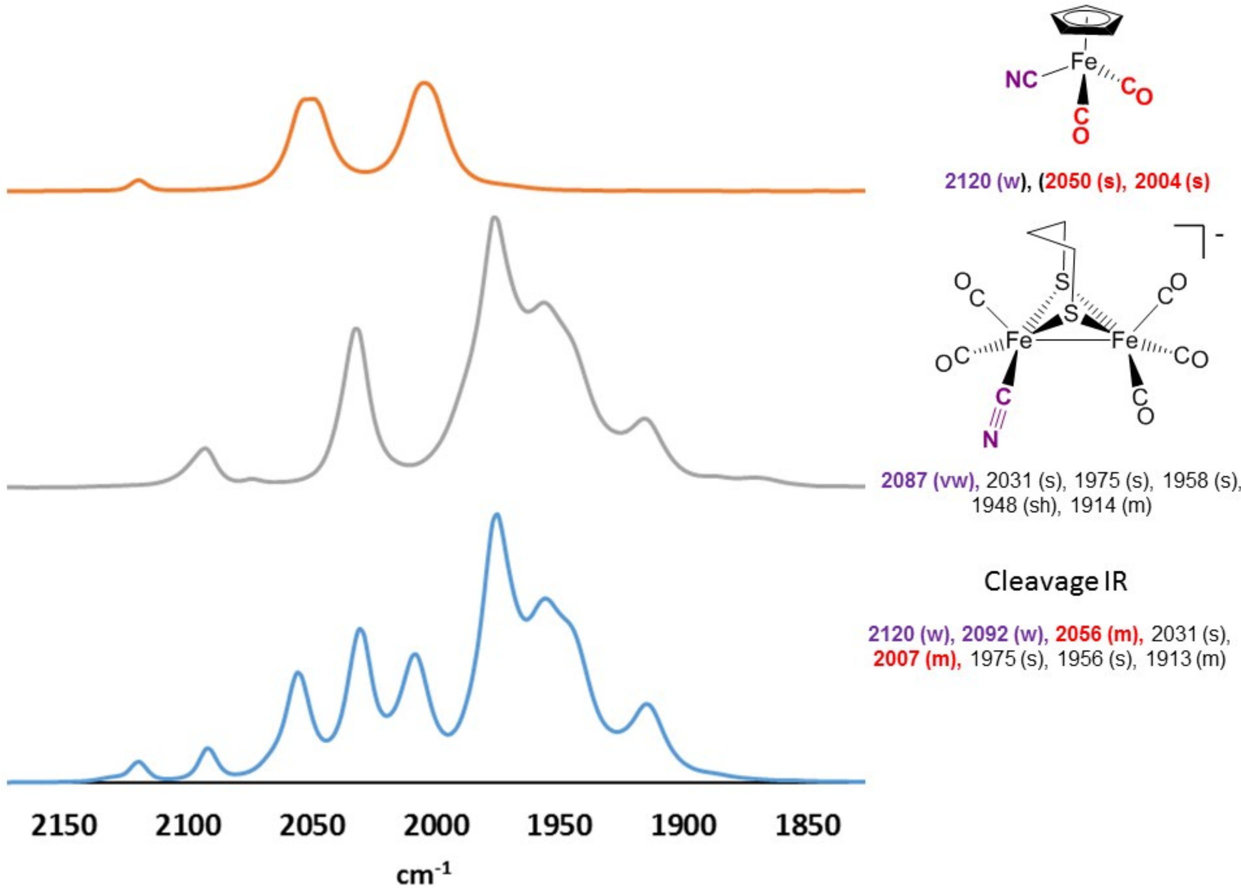

Figure S14. IR spectrum in THF of the cleavage of Compound **A** using tetraethylammonium cyanide.

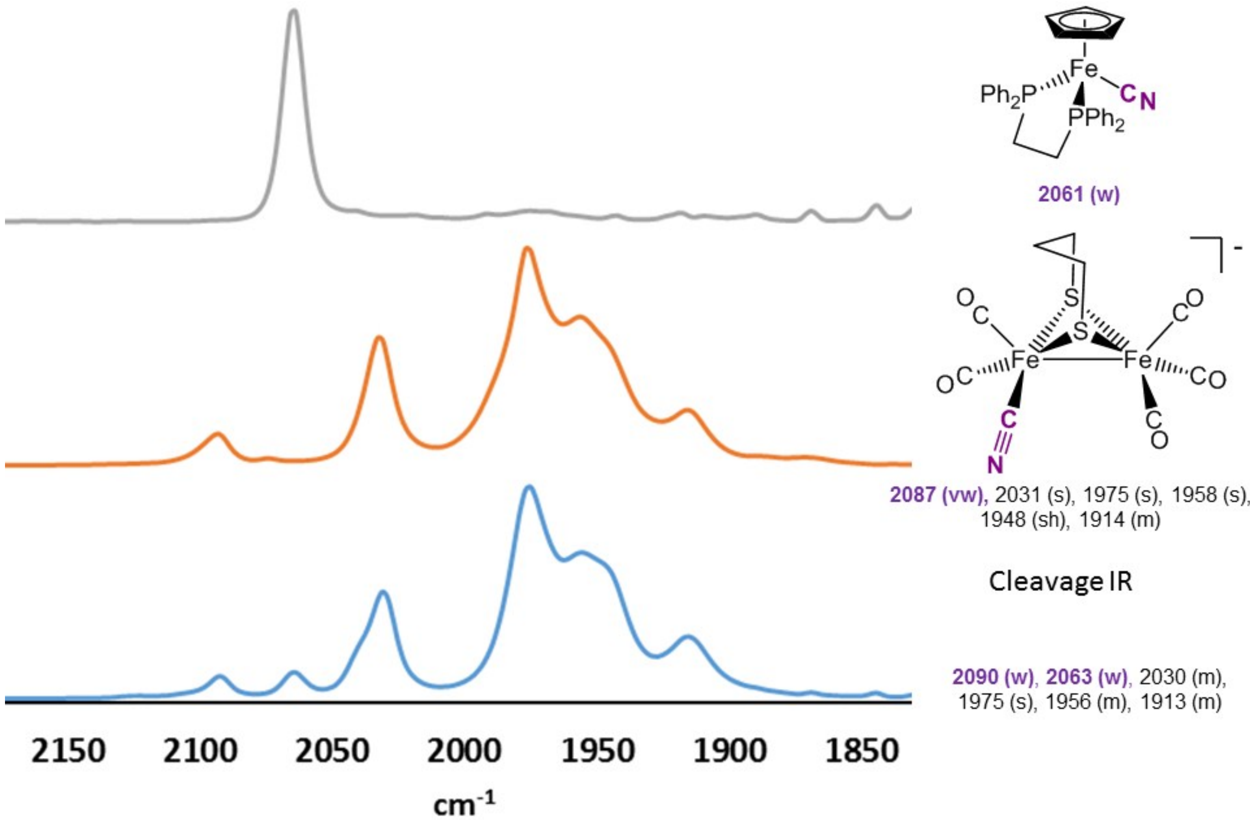

Figure S15. IR spectrum in THF of the cleavage of Compound **B** using PMe_3**.**

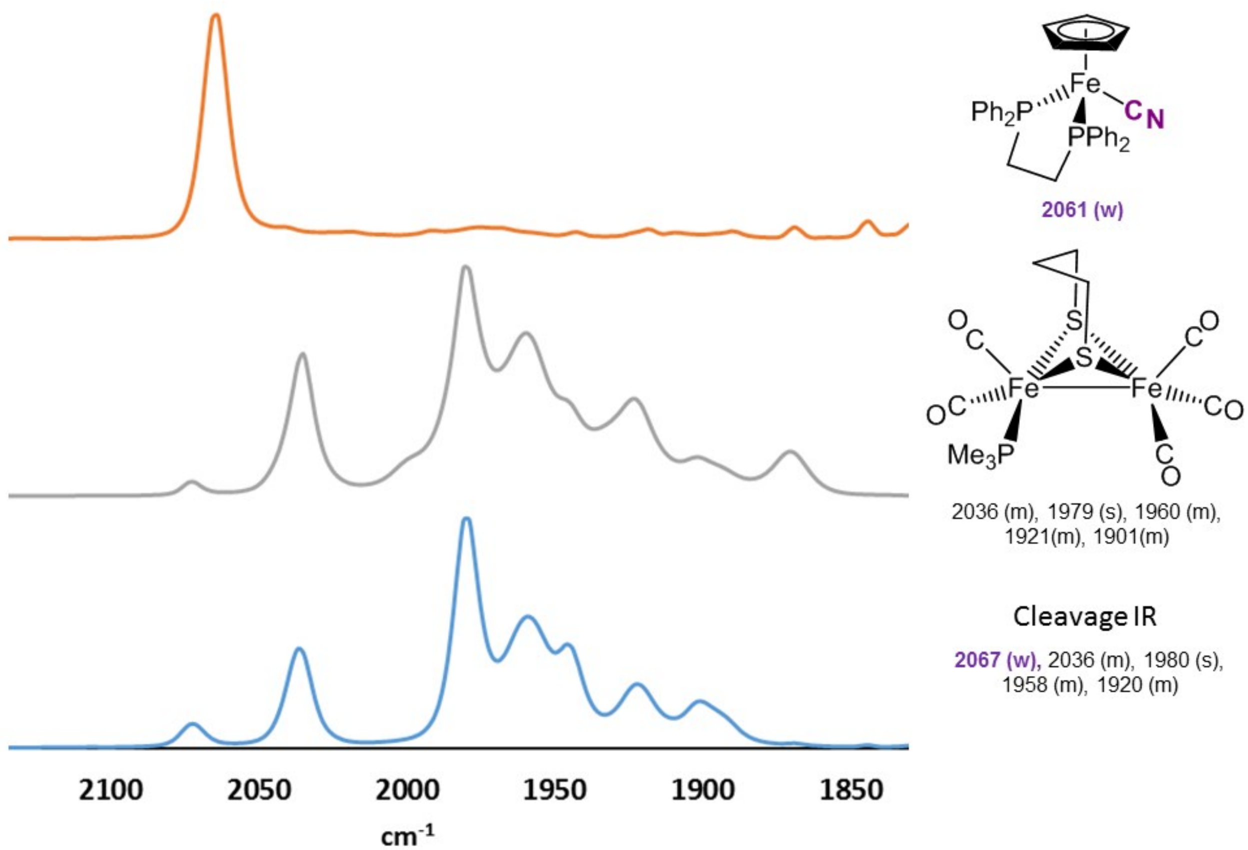

Figure S16. IR spectrum in THF of the cleavage of Compound **B** using tetraethylammonium cyanide.

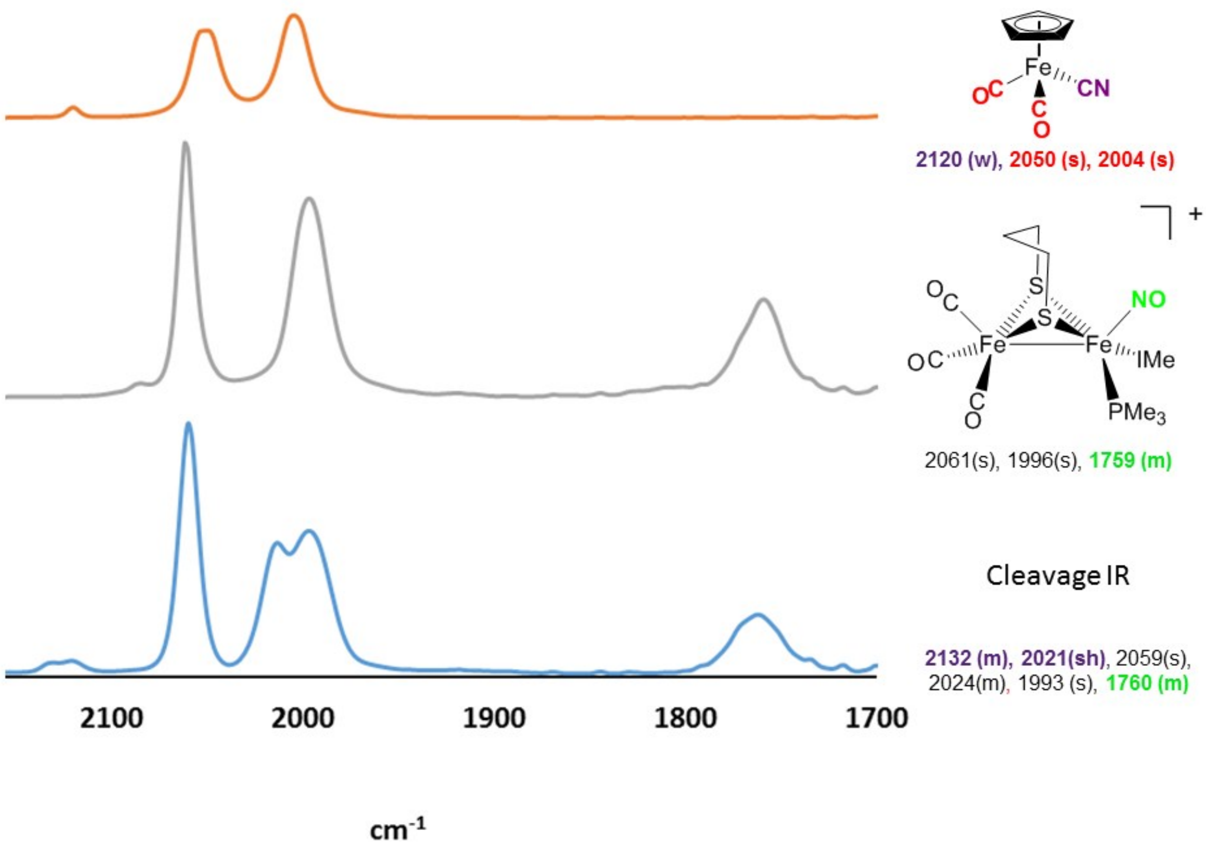

Figure S17. IR spectrum in THF of the cleavage of Compound **C** using PMe_3.

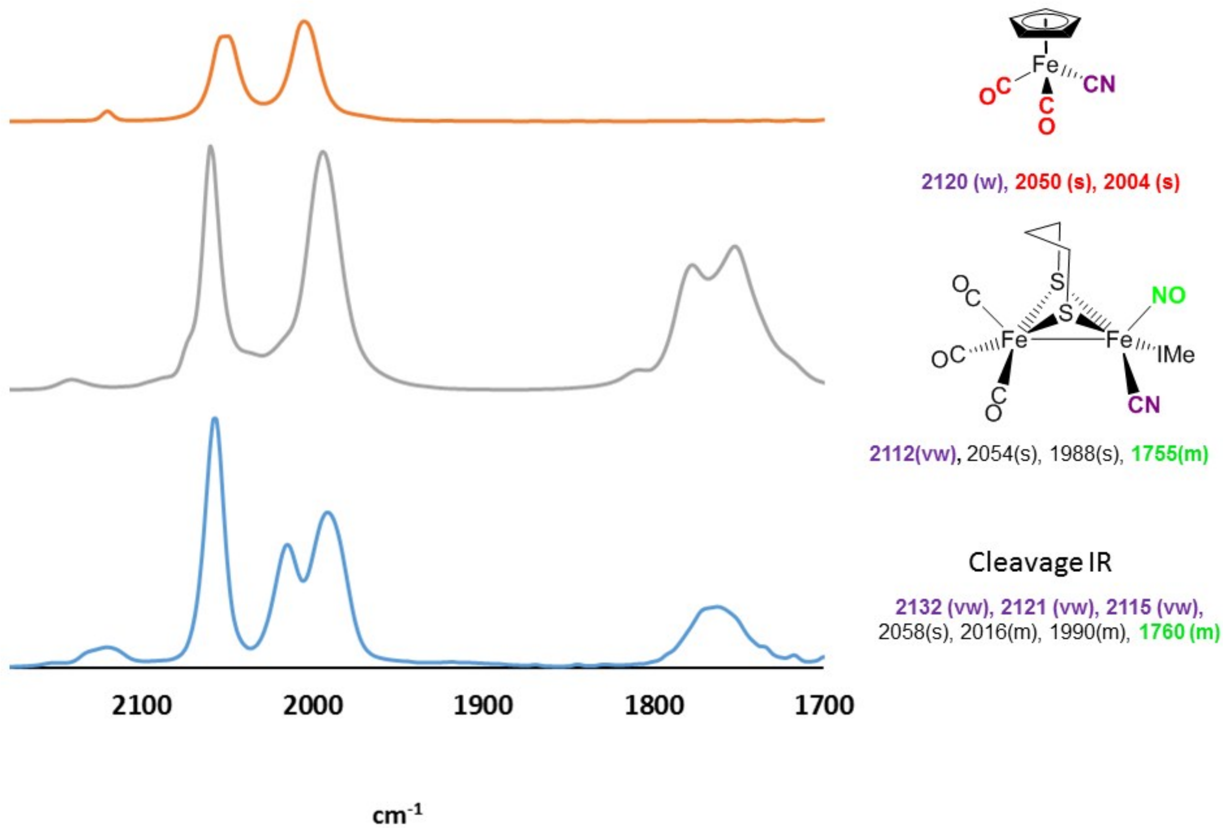

Figure S18. IR spectrum in THF of the cleavage of Compound **C** using tetraethylammonium cyanide.

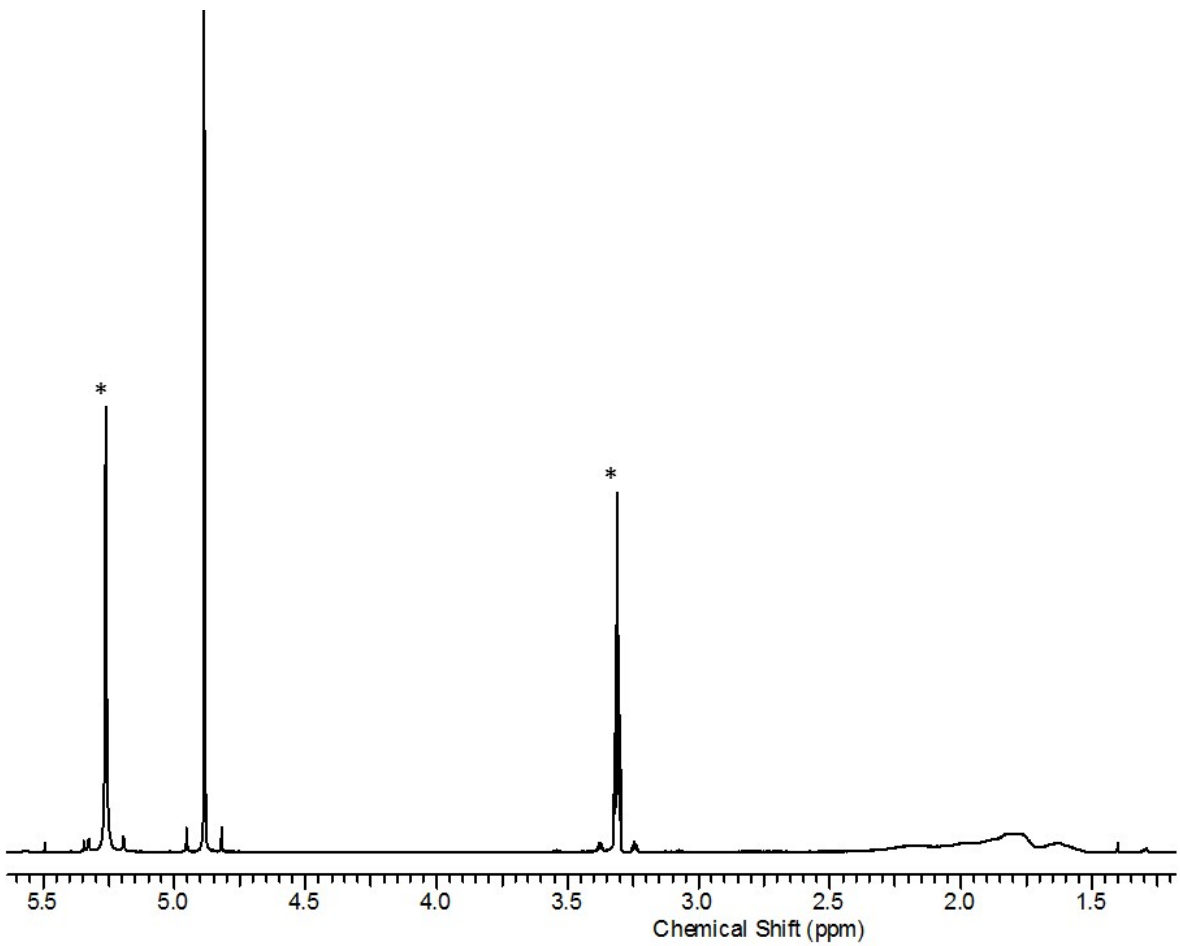

Figure S19. ^{1}H NMR of Compound **A** in CD_3OD. Asterisk denotes residual protonated MeOH.

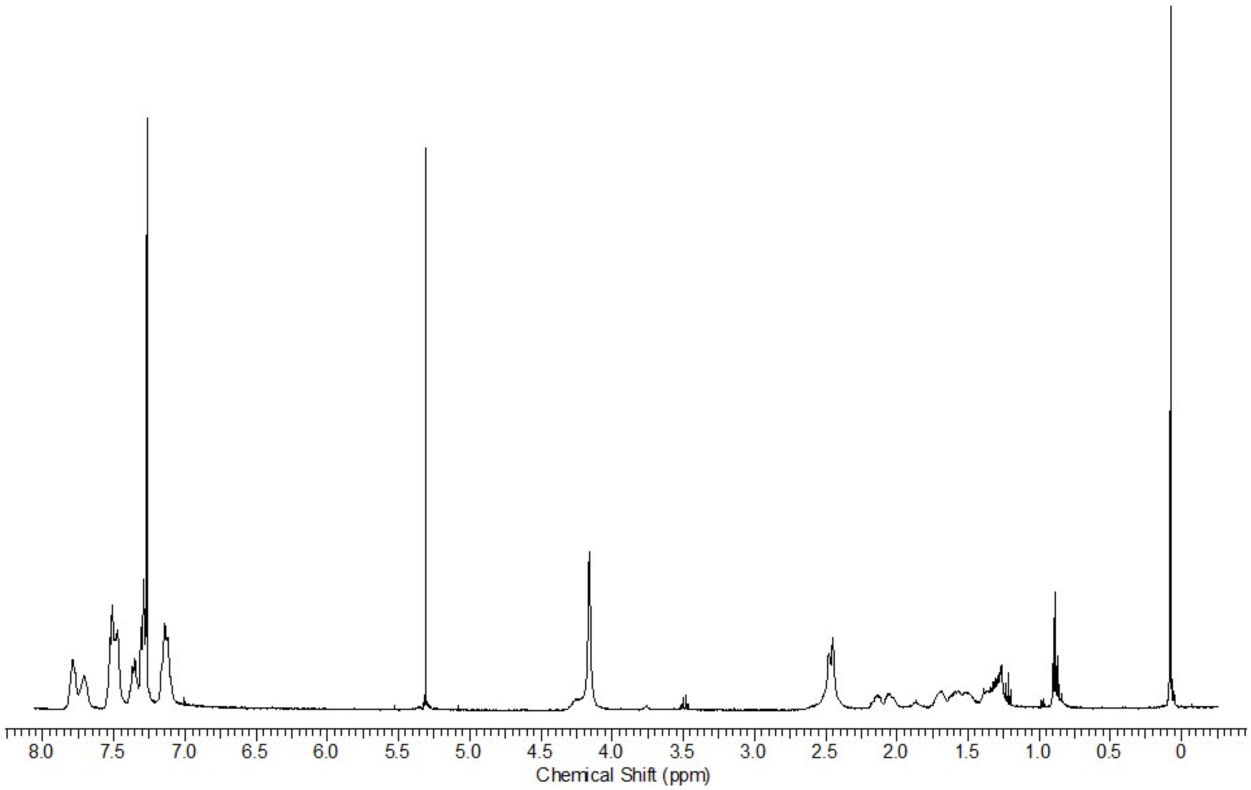

Figure S20. ^{1}H NMR of Compound **B** in $CDCl_3$.

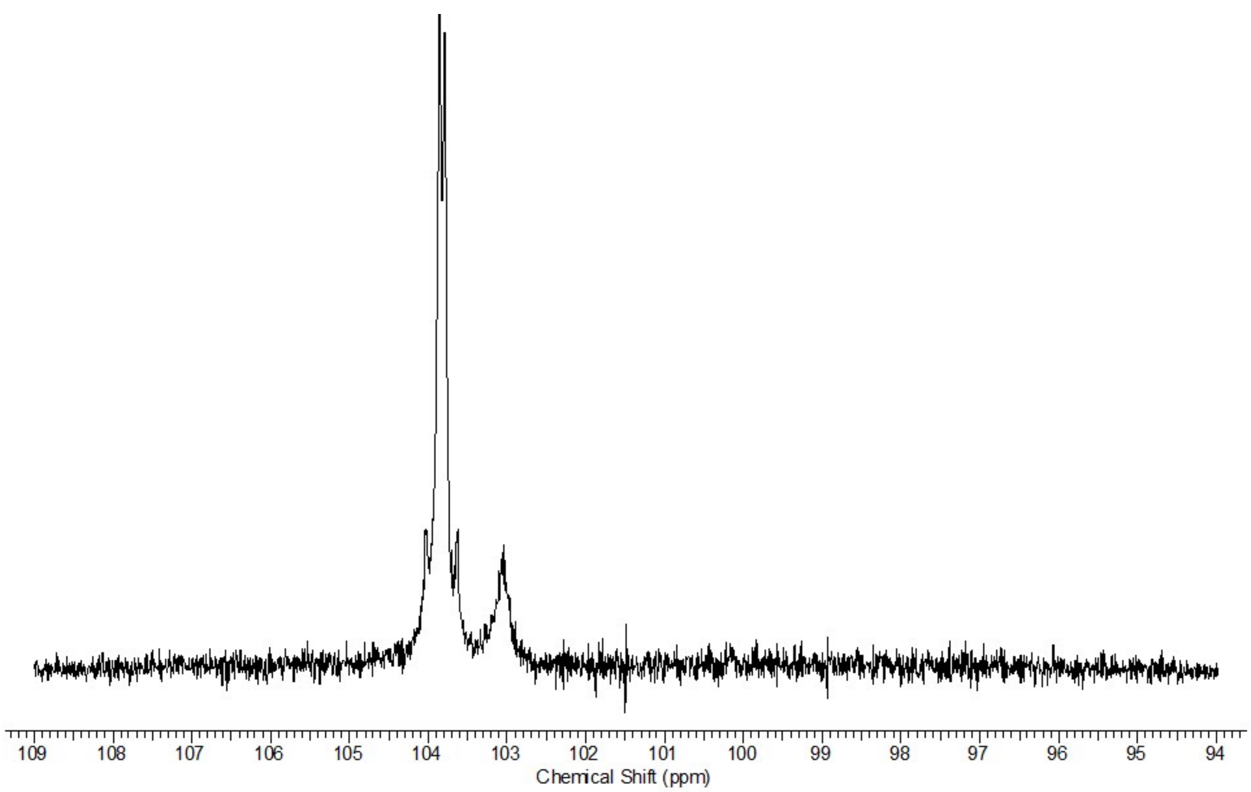

Figure S21. ^{31}P NMR of Compound **B** in $CDCl_3$.

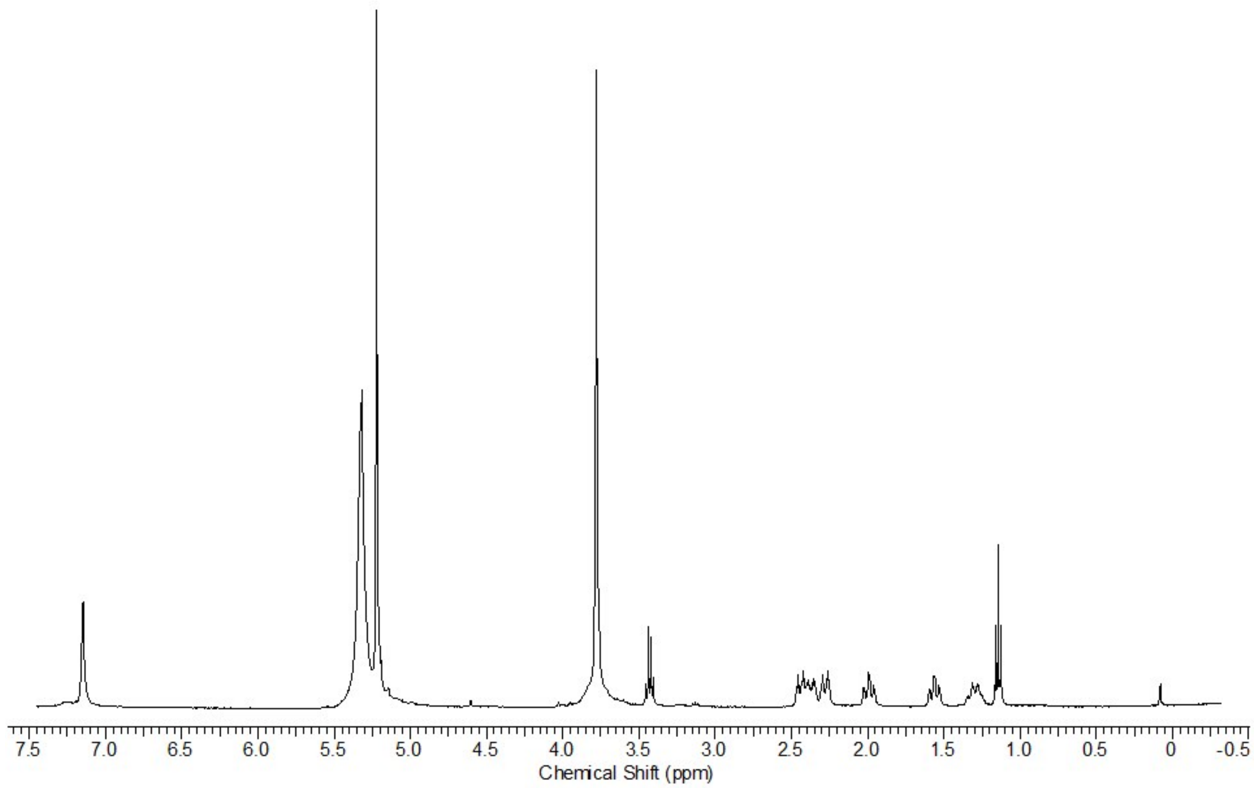

Figure S22. ^{1}H NMR of Compound **C** in CD_2Cl_2.

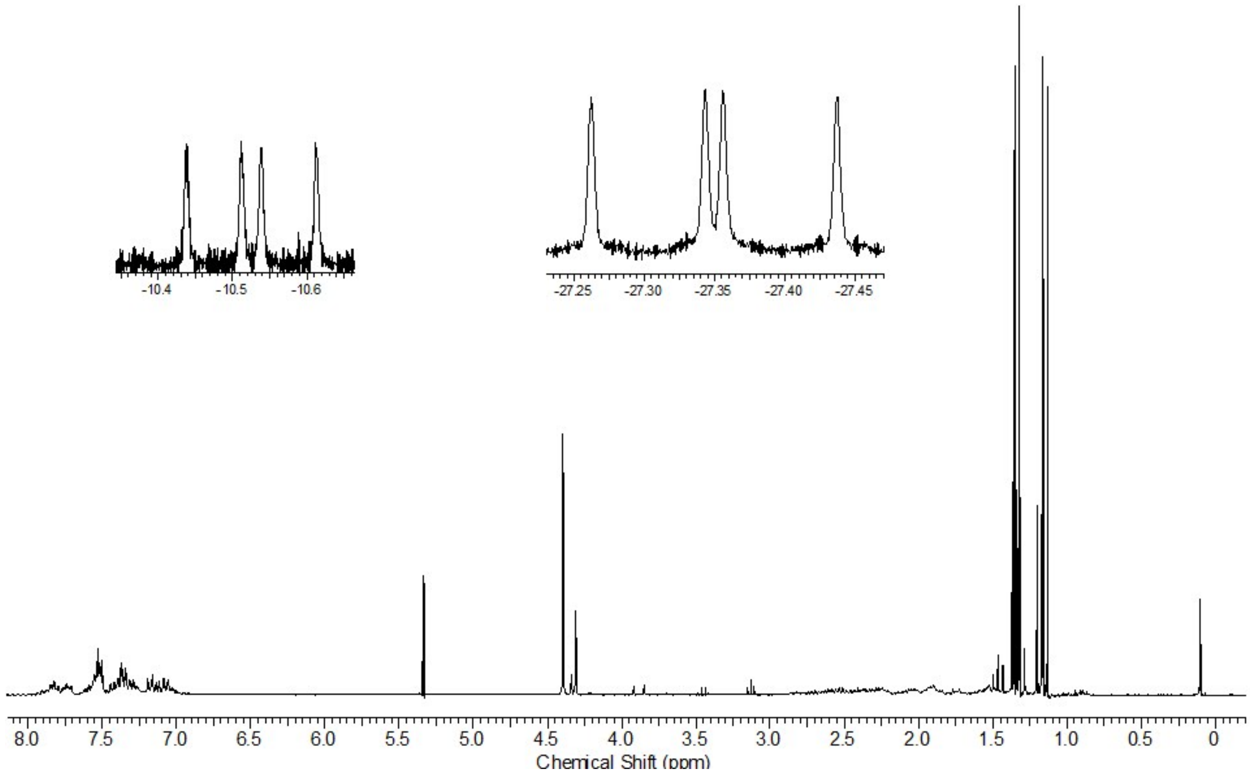

Figure S23. ^1H NMR of Compound **D** in CD_2Cl_2. The hydric upfield region is displayed in the insets.

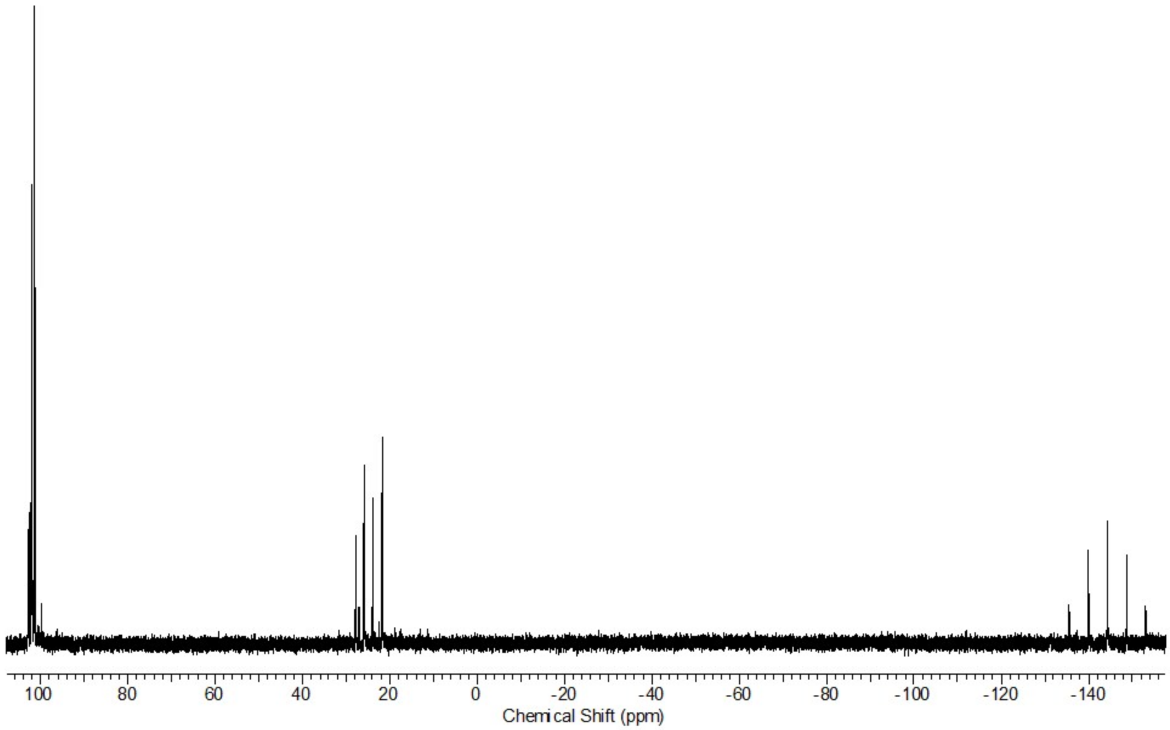

Figure S24. ^{31}P NMR of Compound **D** in CD_2Cl_2

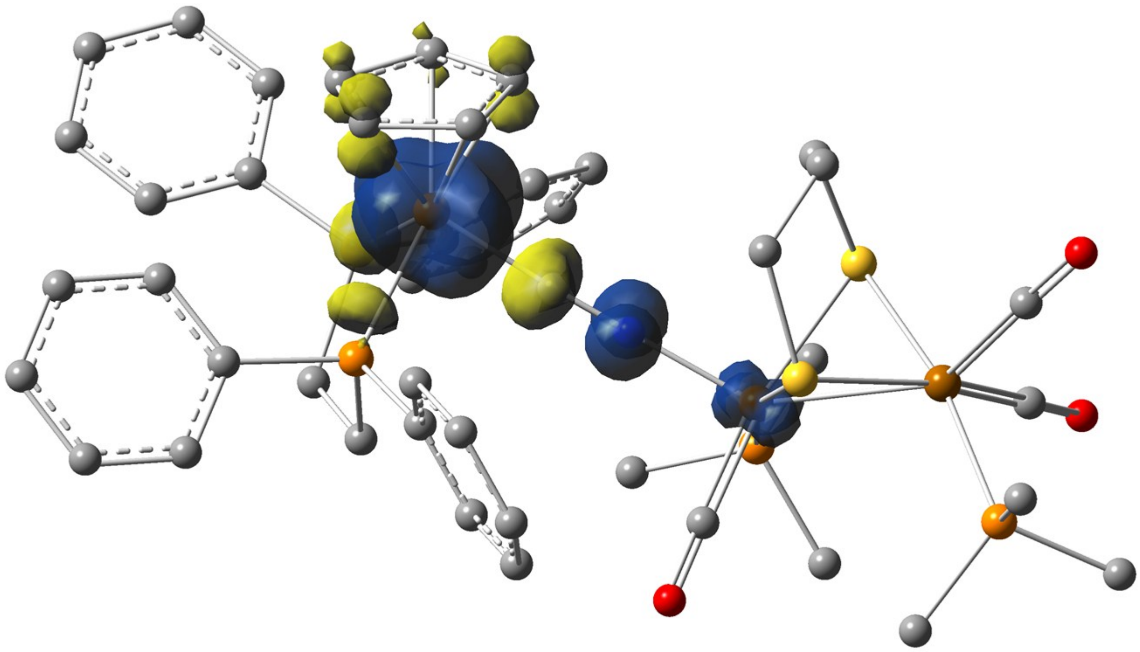

Figure S25. The spin density contour plot of oxidized **D**. (isovalue: 0.0025), calculated by B3LYP. The calculation s show the majority of the unpaired spin is on the iron of the mono-iron moiety, with spin density of 1.163 e, while minor excess spins are on two other irons, bridging cyanide and cyclopentadienyl. The *g* vector was derived from ca lculated *g* tensor and estimated to be (2.018, 2.068 and 2.235). Also see table S3.

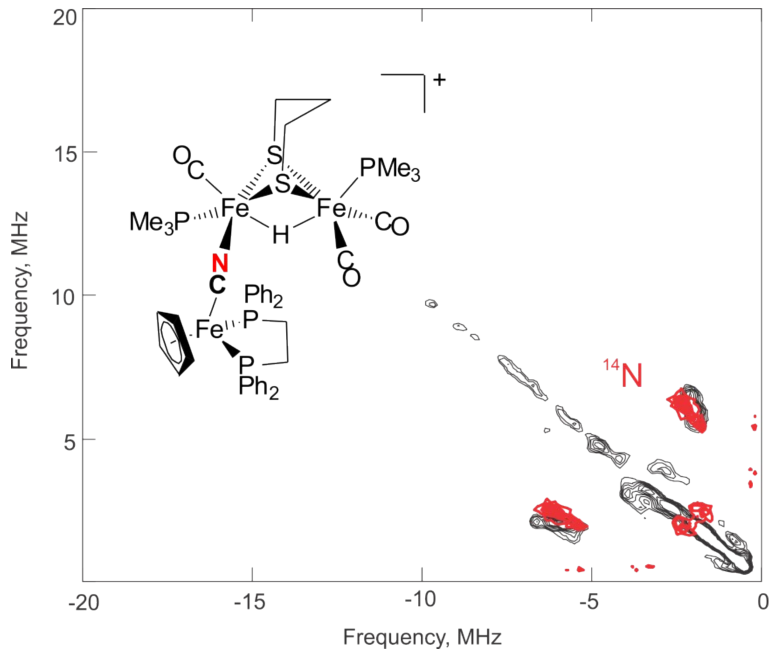

Figure S26. X-band HYSCORE spectrum of electrochemically oxidized (with 0.65 V) complex, **D**$^{+}$, in DCM at 10K. Simulation (in red) parameters (with Easyspin): g (1, 2, 3) = (2.191, 2.089, 2.024); ^{14}N HFC, A_{iso} = 3 MHz, *K* = 0.5; eta = 0.1; tau = 200ns: Field position = 343.8 mT (corresponding to g_2); Micro wave frequency = 9.78651 GHz.

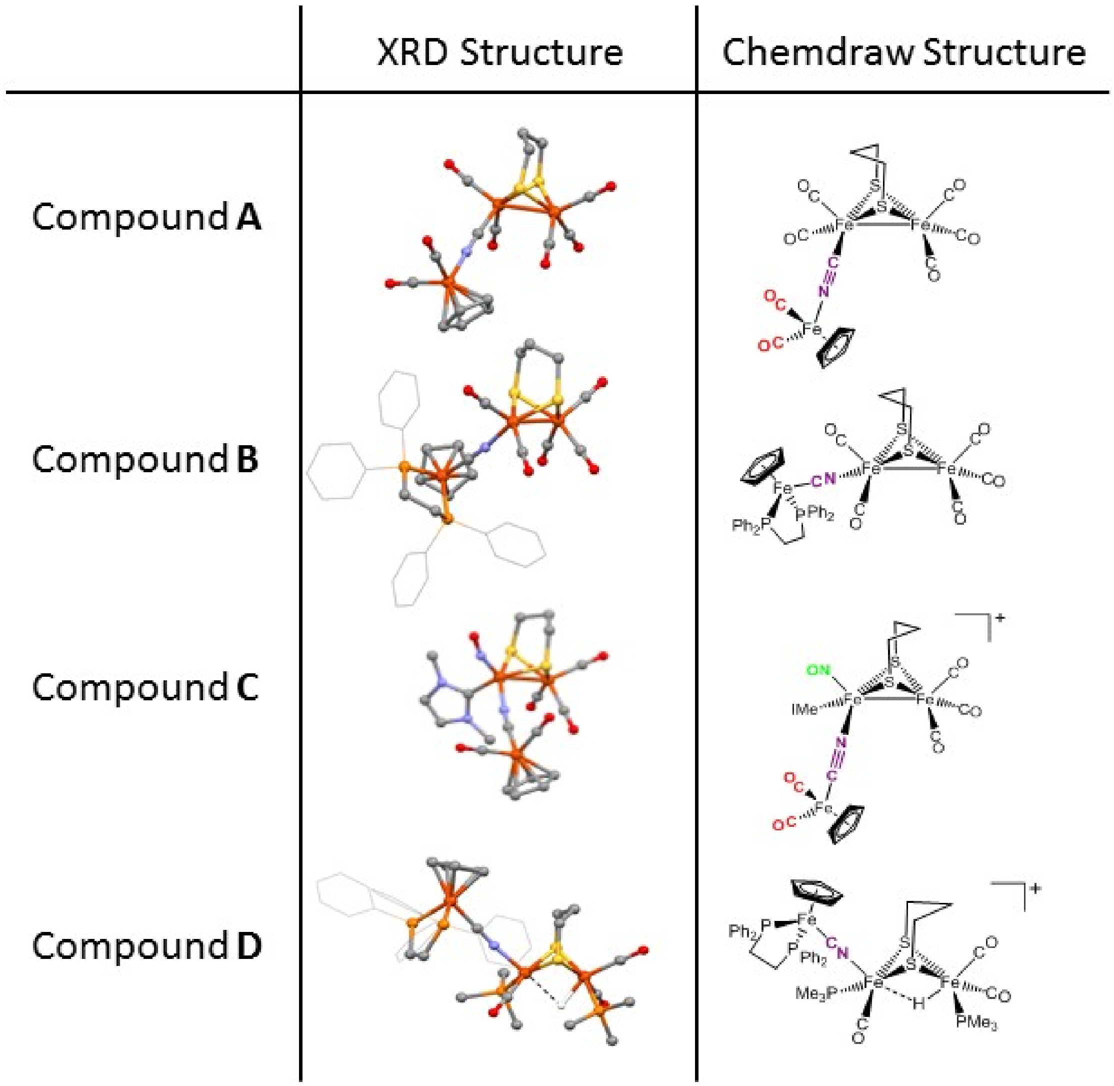

Figure S27. Structures for compounds **A-D** as determined by X-ray diffraction experiments with the analogous chemdraw structures. Hydrogen atoms and counter ions have been omitted for clarity and phenyl rings are in wireframe. Thermal ellipsoid plots are at 50% probability.

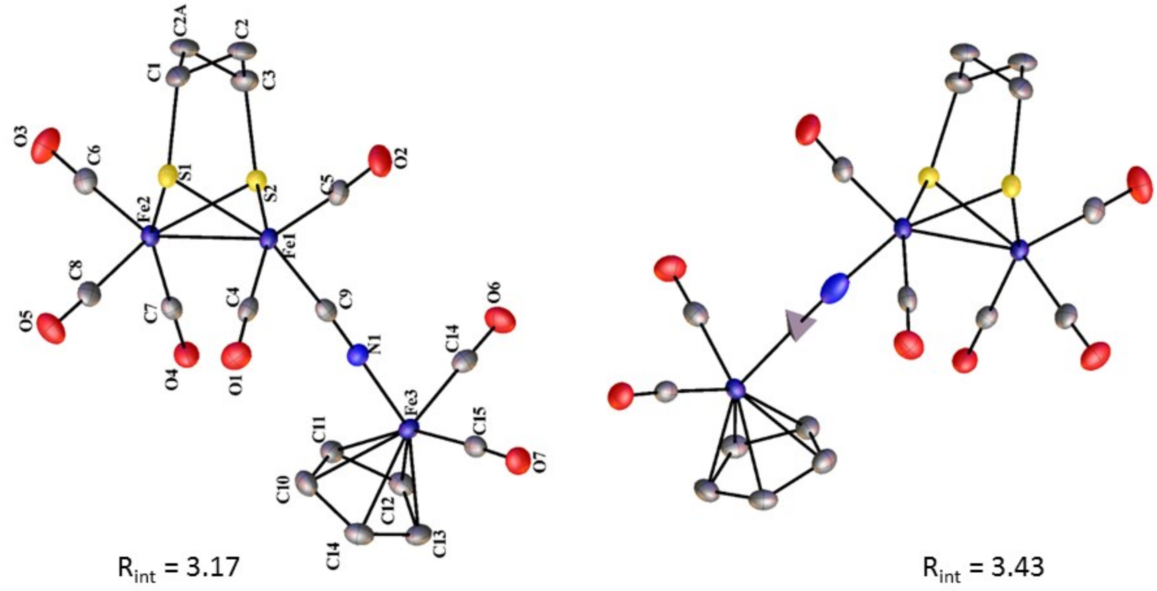

Figure S28. Comparison of the shape of the thermal ellipsoid plots and resulting refinement factor for the two cyanide orientations for Compound **A.** Hydrogens omitted for clarity.

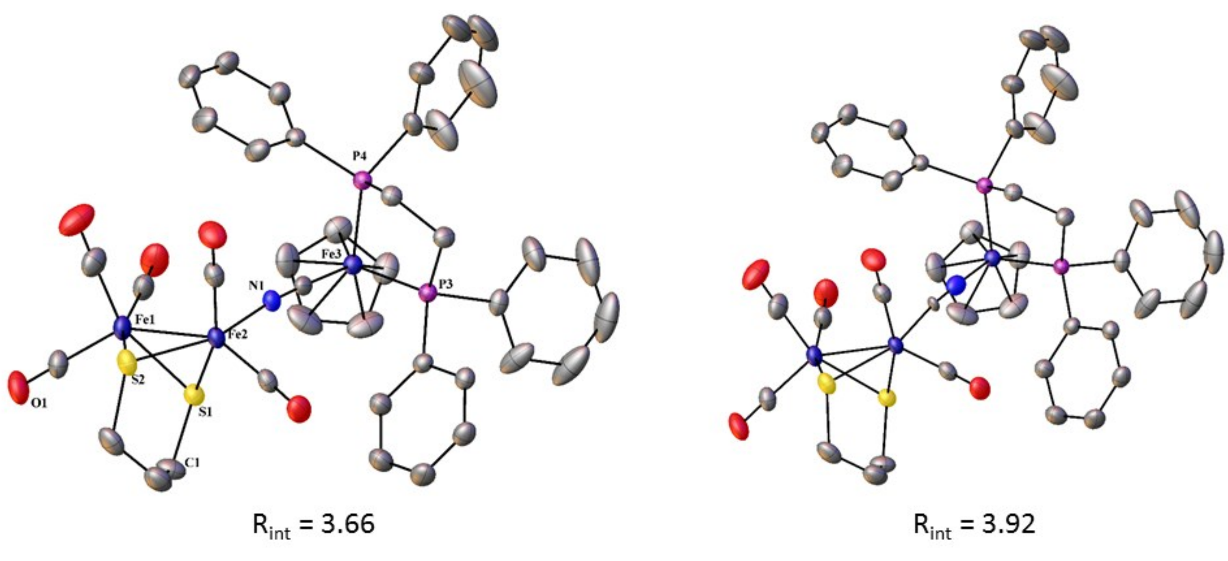

Figure S29. Comparison of the shape of the thermal ellipsoid plots and resulting refinement factor for the two cyanide orientations for Compound **B.** Hydrogens omitted for clarity.

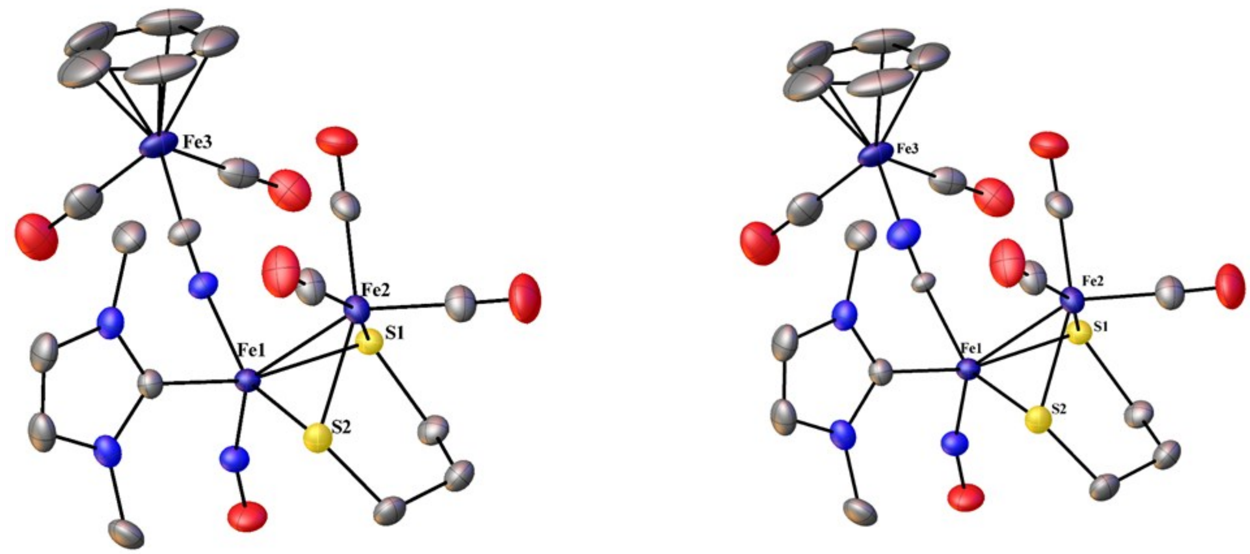

R_{int} = 5.20 R_{int} = 5.38

Figure S30. Comparison of the shape of the thermal ellipsoid plots and resulting refinement factor for the two cyanide orientations for Compound **C**. Counter ions have been omitted for clarity. Hydrogens omitted for clarity.

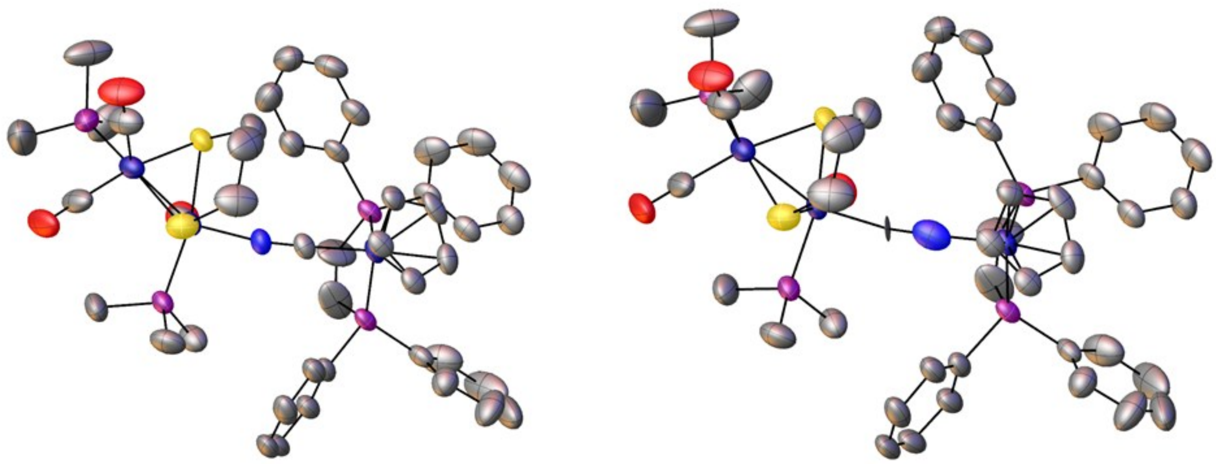

R_{int} = 7.90 R_{int} = 7.94

Figure S31. Comparison of the shape of the thermal ellipsoid plots and resulting refinement factor for the two cyanide orientations for Compound **D**. Counter ions have been omitted for clarity. Hydrogens omitted for clarity.

Table S1. Selected metric data of optimized structures in comparison to experimental values.

Metric data	**Complex A** (Fe-NC-FeFe)			**Complex B** (Fe-CN-FeFe)			**Complex C** (Fe-CN-FeFe)			**Complex D** (Fe-CN-FeFe)		
	Exp.	**Fe-NC-FeFe**	Fe-CN-FeFe	Exp.	Fe-NC-FeFe	**Fe-CN-FeFe**	Exp.	Fe-NC-FeFe	**Fe-CN-FeFe**	Exp	Fe-NC-FeFe	**Fe-CN-FeFe**
Fe-N	1.930	1.911	1.928	1.956	1.921	1.946	1.972	1.919	1.949	1.939	1.936	1.942
N-C	1.152	1.177	1.170	1.158	1.179	1.179	1.147	1.174	1.172	1.172	1.182	1.184
C-Fe	1.917	1.881	1.897	1.876	1.908	1.878	1.900	1.917	1.892	1.887	1.906	1.889
Fe-N-C	177.6	176.2	177.5	170.6	174.8	175.4	171.4	175.3	169.6	171.6	176.0	173.7
N-C-Fe	177.2	177.7	177.5	177.1	177.5	177.0	177.1	172.9	177.9	177.4	175.1	176.0

Comments: Though C and N are similar in electron count and are expected to yield comparable diffractions when examined by X-ray crystallography, the metric data should be reliable regardless of the assignment of C or N. By comparing the differences between FeFe-C/N and Fe-C/N bond lengths, the experimental assignments of complexes **B**-**D** are confirmed by calculations. For complex **A**, the difference is too small to make a judgment.

Table S2. Computational IR frequencies in comparison with experimental values

Complex	Orientation	Vibrational frequency (cm^{-1})		
		CN	NO	CO (Those from monoiron unit are underlined)
A	exp[a]	2128	-	1930, 1955,1986, 2026, 2039, 2069
	Fe-NC-FeFe	2130	-	1947, 1948, 1966, 1986, 2018, 2023, 2058
	Fe-CN-FeFe	2173	-	1944, 1945, 1963, 1986, 2017, 2024, 2055
B	exp	2120	-	1919, 1947, 1980, 2028, 2035
	Fe-NC-FeFe	2102	-	1932, 1954, 1961, 1976, 2021
	Fe-CN-FeFe	2100	-	1929, 1952, 1957, 1975, 2020
C	exp[a]	2154	1755	1995, 2024, 2060, 2067
	Fe-NC-FeFe	2146	1810	1988, 2002, 2023, 2051, 2063
	Fe-CN-FeFe	2155	1795	1986, 2002, 2023, 2051, 2060
D	exp	2081	-	1949, 1964, 2020
	Fe-NC-FeFe	2078	-	1941, 1972, 2016
	Fe-CN-FeFe	2063	-	1939, 1970, 2014

a. The origins of CO frequencies cannot be distinguished solely based on frequencies.

Generally the calculated frequencies match the experimental values with an error less than 20 cm^{-1}. The differences between two linkage isomers are trivial therefore the determination of the structure by IR frequencies is feasible.

Table S3. Experimental and computational EPR parameters for complex D^{+}.

Orientation	Hyperfine constants A_{xyz} (MHz)				Quadrupole Con-stant *K* (MHz)
	Two ^{31}P (*a* = 100 %) on the mono-iron unit		^{13}C (*a* = 1.1 %)	^{14}N (*a* = 99.6 %)	^{14}N (*I* = 1.0)
CW EPR (Exp.)	- 97, -60, -97	-90, -50, -90	Not detected	---	--
HYSCORE (Exp.)*	--	--	--	2, 3, 4	0.5
Fe-NC-FeFe (Calc.)	-76.02, -77.58, -110.43	-76.55, -77.15, -110.67	-0.70, -3.68, 9.88	-8.63, -9.67, -10.19	-0.34
Fe-CN-FeFe (Calc.)	-85.86, -87.37, -122.74	-84.75, -85.72, -120.85	-43.85, -52.11, -59.49	-1.55, -2.27, 7.94	-0.69

The hyperfine coupling of ^{14}N in the Fe-CN-FeFe isomer is calculated to be relatively small as expected because of the distance between N and the spin center (mono-iron unit). The hyperfine coupling of ^{13}C is hard to observe because of the low natural abundance of ^{13}C. The hyperfine coupling constants of ^{31}P match fitted values from simulations to the same extent, regardless of the orientation of CN.

*Simulation parameters are as shown presenting the range of the HFC components. Field dependent HYSCORE is required in order to obtain quantitative anisotropic components of the ^{14}N HFC which was not possible due to sensitivity issues at g_1 and g_3.

Table S4. Energy profiles (Gibbs free energy in kcal/mol) of cyanide flipping with H-bond providers

H-bond provider (P)	Fe-CN-FeFe	Fe-CN-FeFe + P	TS(+ P)	Fe-NC-FeFe + P	Fe-NC-FeFe
None [a]	0	--	34.1	--	1.0
H_2O	0	6.0	34.3	7.5	1.0
$(H_2O)_2$	0	9.8	43.2	12.1	1.0
Urea	0	4.2	39.4	6.0	1.0
Hpy^+	0	2.8	36.1	4.8	1.0

a. In addition to thermal and solvation corrections, empirical dispersion (GD3BJ) is also added to fully evaluate the contributions from possible H-bonds. Therefore the values of the CN-bridged complexes are slightly different from those in the text without the dispersion.

Table S5. Crystal data and structure refinement for Compound **A**

Identification code	cn	
Empirical formula	C16 H11 Fe3 N O7 S2	
Formula weight	560.93	
Temperature	110.15 K	
Wavelength	0.71073 Å	
Crystal system	Triclinic	
Space group	P -1	
Unit cell dimensions	a = 7.7263(14) Å	α= 94.504(10)°.
	b = 11.203(2) Å	β= 108.019(10)°.
	c = 11.900(2) Å	γ = 93.687(10)°.
Volume	972.3(3) $Å^3$	
Z	2	
Density (calculated)	1.916 Mg/m^3	
Absorption coefficient	2.463 mm^{-1}	
F(000)	560	
Crystal size	0.12 x 0.1 x 0.08 mm^3	
Theta range for data collection	1.809 to 27.575°.	
Index ranges	-10<=h<=9, -14<=k<=14, 0<=l<=15	
Reflections collected	4458	
Independent reflections	4458 [R(int) = ?]	
Completeness to theta = 25.242°	99.7 %	
Absorption correction	Semi-empirical from equivalents	
Max. and min. transmission	0.745 and 0.581	
Refinement method	Full-matrix least-squares on F^2	
Data / restraints / parameters	4458 / 6 / 267	
Goodness-of-fit on F^2	1.051	
Final R indices [I>2sigma(I)]	R1 = 0.0317, wR2 = 0.0756	
R indices (all data)	R1 = 0.0380, wR2 = 0.0788	
Extinction coefficient	n/a	
Largest diff. peak and hole	0.516 and -0.467 e.$Å^{-3}$	

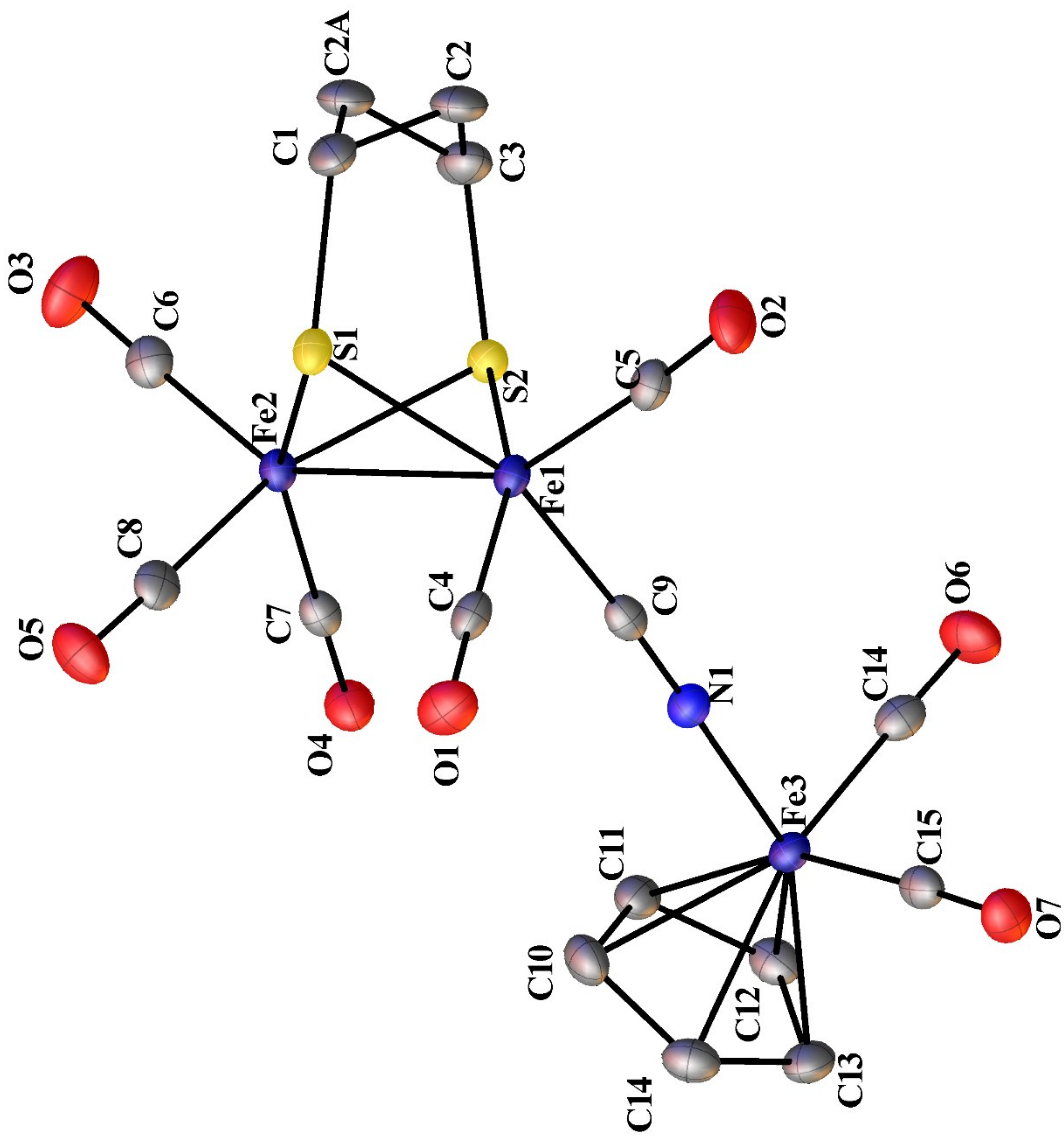

Figure S32. Thermal ellipsoid plot at 50% probability for Compound **A**. Hydrogens omitted for clarity.

Table S6. Crystal data and structure refinement for Compound **B**.

Identification code	pdtisomer	
Empirical formula	C40 H35 Fe3 N O5 P2 S2	
Formula weight	903.30	
Temperature	150.15 K	
Wavelength	0.71073 Å	
Crystal system	Triclinic	
Space group	P-1	
Unit cell dimensions	a = 11.3103(15) Å	α= 105.449(5)°.
	b = 12.9416(18) Å	β= 100.216(5)°.
	c = 15.479(2) Å	γ = 110.921(4)°.
Volume	1944.2(5) $Å^3$	
Z	2	
Density (calculated)	1.543 Mg/m^3	
Absorption coefficient	1.339 mm^{-1}	
F(000)	924	
Crystal size	0.15 x 0.14 x 0.1 mm^3	
Theta range for data collection	2.023 to 27.898°.	
Index ranges	-14<=h<=14, -16<=k<=16, -20<=l<=20	
Reflections collected	87852	
Independent reflections	9112 [R(int) = 0.0396]	
Completeness to theta = 25.242°	99.9 %	
Absorption correction	Semi-empirical from equivalents	
Max. and min. transmission	0.7456 and 0.6533	
Refinement method	Full-matrix least-squares on F^2	
Data / restraints / parameters	9112 / 90 / 478	
Goodness-of-fit on F^2	1.037	
Final R indices [I>2sigma(I)]	R1 = 0.0366, wR2 = 0.0864	
R indices (all data)	R1 = 0.0469, wR2 = 0.0946	
Extinction coefficient	n/a	
Largest diff. peak and hole	1.370 and -0.472 e.$Å^{-3}$	

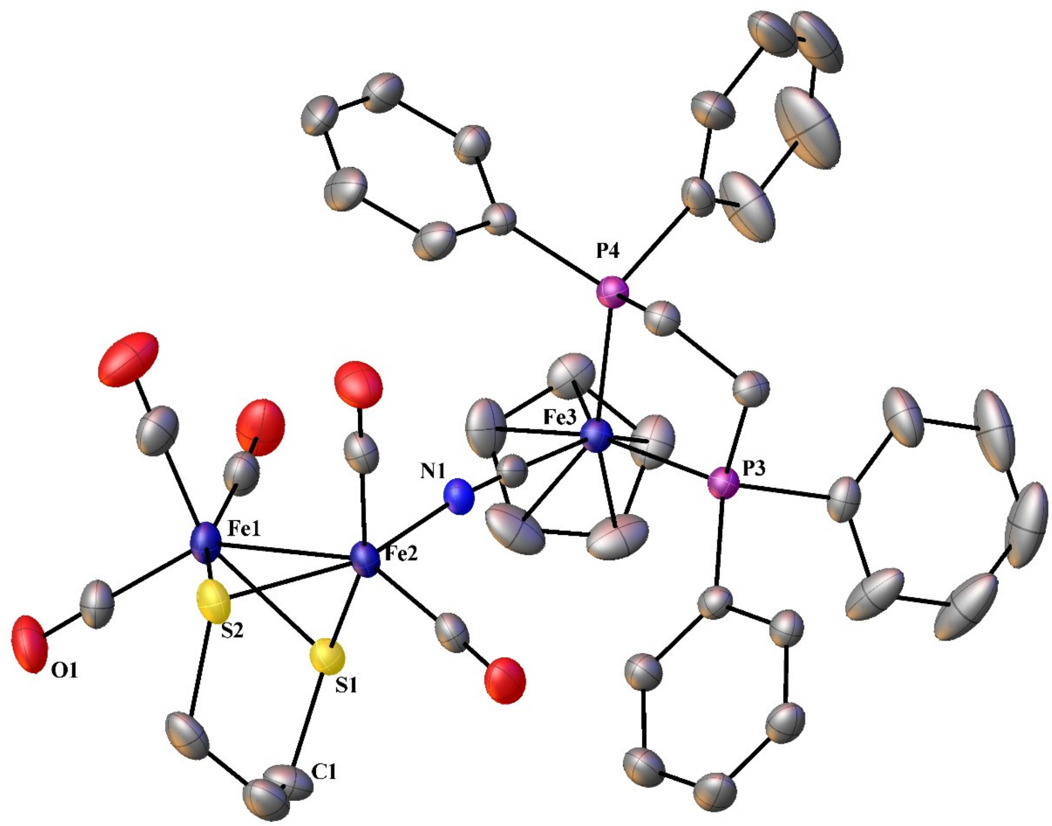

Figure S33. Thermal ellipsoid plot at 50% probability for **B**. Hydrogens omitted for clarity.

Table S7. Crystal data and structure refinement for Compound **C**.

Identification code	8314	
Empirical formula	C20.20 H22.23 B F4 Fe3 N4.60 O6.72 S2	
Formula weight	755.40	
Temperature	110.15 K	
Wavelength	0.71073 Å	
Crystal system	Triclinic	
Space group	P-1	
Unit cell dimensions	a = 10.4593(5) Å	α= 76.988(2)°.
	b = 11.6085(6) Å	β= 85.341(2)°.
	c = 12.2560(6) Å	γ = 81.750(2)°.
Volume	1433.02(12) Å^3	
Z	2	
Density (calculated)	1.751 Mg/m^3	
Absorption coefficient	1.717 mm^{-1}	
F(000)	761	
Crystal size	0.142 x 0.10 x 0.038 mm^3	
Theta range for data collection	1.970 to 30.797°.	
Index ranges	-14<=h<=14, -16<=k<=16, -17<=l<=17	
Reflections collected	46532	
Independent reflections	8411 [R(int) = 0.0436]	
Completeness to theta = 25.242°	99.8 %	
Absorption correction	Semi-empirical from equivalents	
Max. and min. transmission	0.7461 and 0.6145	
Refinement method	Full-matrix least-squares on F^2	
Data / restraints / parameters	8411 / 66 / 369	
Goodness-of-fit on F^2	1.055	
Final R indices [I>2sigma(I)]	R1 = 0.0520, wR2 = 0.1487	
R indices (all data)	R1 = 0.0658, wR2 = 0.1629	
Extinction coefficient	n/a	
Largest diff. peak and hole	2.007 and -1.856 e.Å^{-3}	

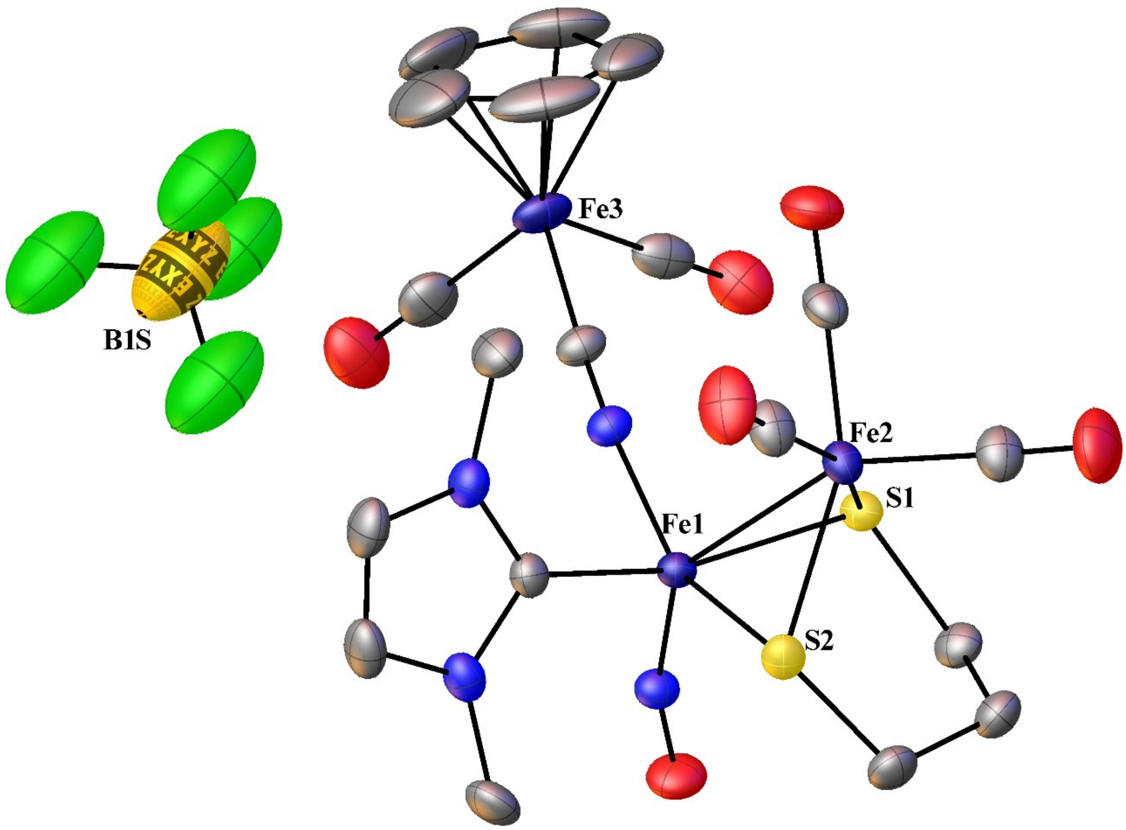

Figure S34. Thermal ellipsoid plot at 50% probability for **C**. Hydrogens omitted for clarity.

Table S8. Crystal data and structure refinement for Compound **D**.

Identification code	twin4	
Empirical formula	C80 H75 B F24 Fe3 N O4 P4 S2	
Formula weight	1936.77	
Temperature	150.15 K	
Wavelength	0.71073 Å	
Crystal system	Triclinic	
Space group	P-1	
Unit cell dimensions	a = 13.352(5) Å	α= 92.828(5)°.
	b = 13.623(5) Å	β= 94.410(5)°.
	c = 24.074(8) Å	γ = 99.584(5)°.
Volume	4296(3) $Å^3$	
Z	2	
Density (calculated)	1.497 Mg/m^3	
Absorption coefficient	0.723 mm^{-1}	
F(000)	1970	
Crystal size	0.15 x 0.09 x 0.08 mm^3	
Theta range for data collection	2.138 to 23.850°.	
Index ranges	?<=h<=?, ?<=k<=?, ?<=l<=?	
Reflections collected	?	
Independent reflections	13129 [R(int) = ?]	
Completeness to theta = 25.242°	84.5 %	
Absorption correction	Semi-empirical from equivalents	
Max. and min. transmission	0.744 and 0.622	
Refinement method	Full-matrix least-squares on F^2	
Data / restraints / parameters	13129 / 0 / 1080	
Goodness-of-fit on F^2	1.082	
Final R indices [I>2sigma(I)]	R1 = 0.0790, wR2 = 0.2135	
R indices (all data)	R1 = 0.1091, wR2 = 0.2317	
Extinction coefficient	n/a	
Largest diff. peak and hole	2.070 and -0.534 e.$Å^{-3}$	

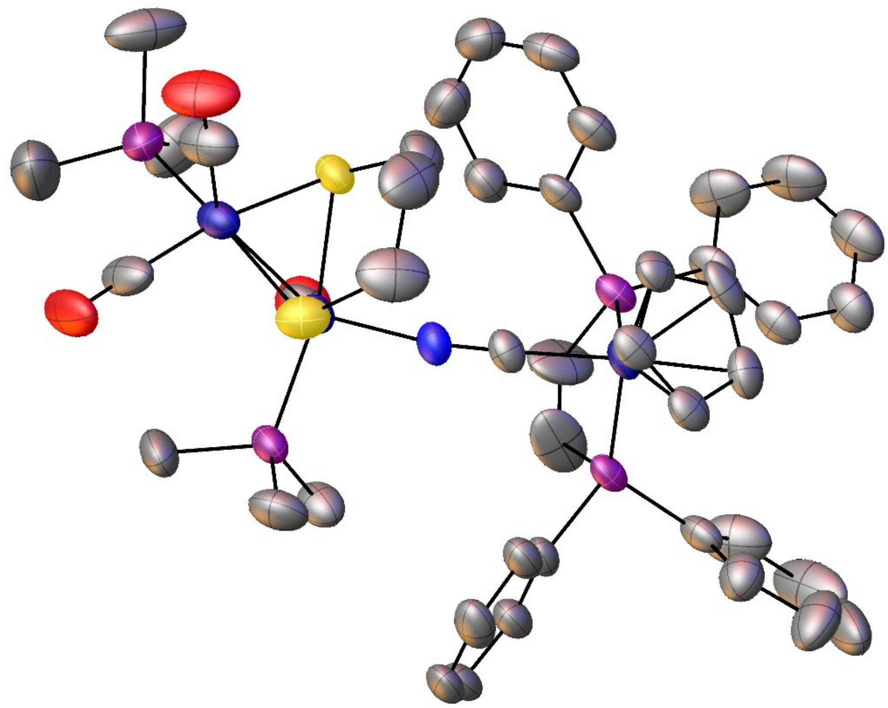

Figure S35. Thermal ellipsoid plot at 50% probability for **D**. Hydrogens and counter ion omitted for clarity.